Applied Catalysis B: Environment and Energy 398 (2026) 127014

Contents lists available at ScienceDirect

Applied Catalysis B: Environment and Energy

journal homepage: www.elsevier.com/locate/apcatb

Artificial Intelligence-driven mechanistic insights in electrocatalysis

Jiwon Kim [a,b,1], Sangkyu Woo [b,1], Hun-Gi Jung [c,d,e,*], Jongsoon Kim [f,g,**], Junyoung Mun [b,g,***], Jung Ho Kim [a,****]

[a] Institute for Superconducting and Electronic Materials (ISEM), Australian Institute for Innovative Materials, University of Wollongong, Squires Way, North Wollongong, NSW 2500, Australia
[b] School of Advanced Materials Science and Engineering, Sungkyunkwan University (SKKU), 2066 Seobu-ro, Jangan-gu, Suwon 16419, Republic of Korea
[c] Energy Storage Research Center, Sustainable Energy Research Division, Korea Institute of Science and Technology, Seoul 02792, Republic of Korea
[d] Division of Energy & Environment Technology, KIST School, Korea University of Science and Technology, Seoul 02792, Republic of Korea
[e] Department of Energy Science and KIST-SKKU Carbon-Neutral Research Center, Sungkyunkwan University, Suwon 16419, Republic of Korea
[f] Department of Energy Science and Department of Energy, Sungkyunkwan University (SKKU), 2066 Seobu-ro, Jangan-gu, Suwon 16419, Republic of Korea
[g] SKKU Institute of Energy Science and Technology (SIEST), Sungkyunkwan University, 2066 Seobu-ro, Jangan-gu, Suwon 16419, Republic of Korea

ARTICLE INFO

Keywords:
Electrocatalysis
Artificial Intelligence
Operando analysis
Atomistic simulation
Mechanistic insight

ABSTRACT

Understanding electrocatalytic mechanisms is essential for rational catalyst design. While operando experiments and atomistic simulations provide complementary insights into catalytic states, they face inherent limitations in resolving dynamically evolving structures, disentangling overlapping signals, and sampling the vast configurational space governing reaction pathways. Here, we present an artificial intelligence (AI)-integrated framework for mechanistic studies in electrocatalysis, positioning AI as a tool to augment and connect conventional approaches. By defining the functional roles of AI in representation, exploration, and inference, we outline how complex operando data can be systematically interpreted, how simulation space can be extended, and how mechanistic hypotheses can be evaluated under physical constraints. Together, this framework offers a structured perspective on integrating AI into mechanistic analysis, highlighting key opportunities and limitations, and establishing a conceptual pathway toward a more consistent, mechanism-driven understanding of electrocatalytic systems.

1. Introduction

In heterogeneous electrocatalysis, catalytic reactions occur at solid–liquid interfaces under applied potential, where catalyst structure and the electrochemical environment are inherently coupled [1,2]. Thus, electrocatalytic behavior is governed not by static material properties but by the evolving states of active sites, reaction intermediates, and the surrounding environment during operation [3–5]. Mechanistic understanding is therefore essential for establishing causal relationships between catalyst structure, reaction conditions, and macroscopic performance [6,7]. However, resolving electrocatalytic mechanisms remains challenging because these coupled factors evolve dynamically under non-equilibrium conditions [1,5]. Catalysts undergo continuous structural and electronic changes, while intermediates form, decay, and compete on short time scales [8–14]. In addition, electrolyte composition, solvation structure, and interfacial electric fields actively modulate reaction pathways and selectivity [15–17]. This intrinsic, time-dependent complexity fundamentally limits mechanistic descriptions based on static structures or equilibrium assumptions.

Electrocatalytic reactions are commonly investigated using a combination of operando experiments and atomistic simulations [18–22]. Operando electrocatalytic techniques enable direct observation of

* Corresponding author at: Energy Storage Research Center, Sustainable Energy Research Division, Korea Institute of Science and Technology, Seoul 02792, Republic of Korea.
** Corresponding author at: Department of Energy Science and Department of Energy, Sungkyunkwan University (SKKU), 2066 Seobu-ro, Jangan-gu, Suwon 16419, Republic of Korea.
*** Corresponding author at: School of Advanced Materials Science and Engineering, Sungkyunkwan University (SKKU), 2066 Seobu-ro, Jangan-gu, Suwon 16419, Republic of Korea.
**** Corresponding author.
E-mail addresses: hungi@kist.re.kr (H.-G. Jung), jongsoonkim@skku.edu (J. Kim), munjy@skku.edu (J. Mun), jhk@uow.edu.au (J.H. Kim).
[1] J. Kim and S. Woo contributed equally to this work

https://doi.org/10.1016/j.apcatb.2026.127014
Received 28 February 2026; Received in revised form 7 May 2026; Accepted 24 May 2026
Available online 26 May 2026

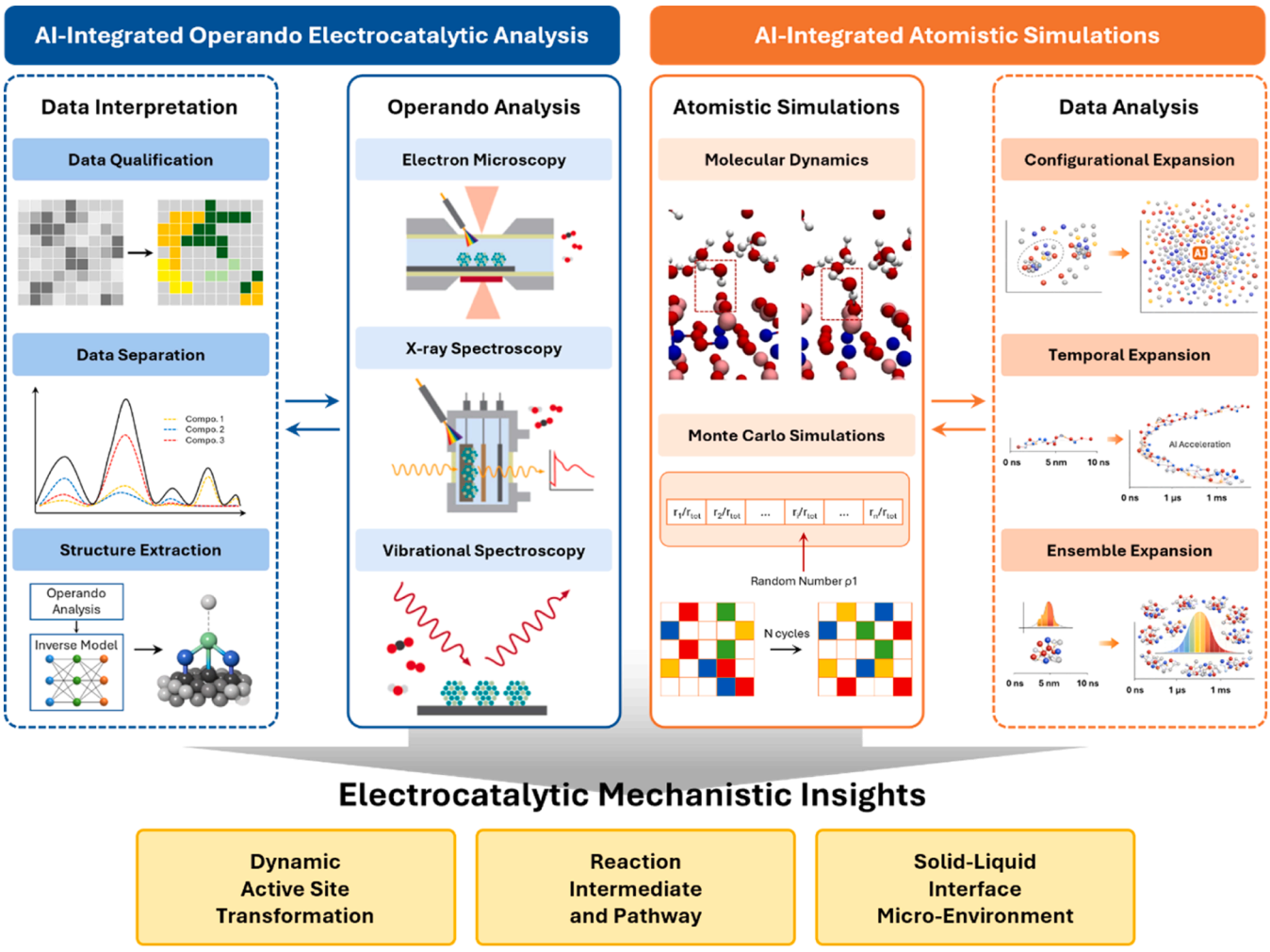

Fig. 1. Conceptual overview of AI-integrated mechanistic analysis in electrocatalysis. Reproduced with permission from Ref. [33]. Copyright 2025 American Chemical Society. Reproduced with permission from Ref. [40]. Copyright 2023 John Wiley and Sons.

catalysts under working conditions, providing insight into dynamic structural transformations, changes in electronic states, and the formation of surface-bound reaction intermediates [23–25]. Atomistic simulations offer a complementary molecular-level perspective for interpreting reaction energetics, reaction pathways, and environment-mediated effects [26–28]. Together, these experimental and computational approaches form the foundation of mechanistic understanding in electrocatalysis by linking observable catalyst dynamics to underlying reaction processes. However, when applied to complex and dynamic electrocatalytic systems, both approaches face inherent challenges in data interpretation, mechanistic resolution, and efficient exploration of relevant reaction space, motivating the development of new integrative strategies [29–31].

To address these limitations, AI is emerging as a promising set of data-driven tools for electrocatalytic mechanism studies [32–36]. Rather than representing physical models or experimental analysis, AI is being explored to assist the interpretation of complex operando measurements and the exploration of mechanistic space in atomistic simulations. By extracting structure, patterns, and relationships from high-dimensional data, AI enables the organization of evolving catalyst states, reaction intermediates, and reaction environments into interpretable representations [37–39]. Although these approaches are not yet routine, their conceptual alignment with the demands of operando electrocatalysis and molecular simulations hold significant promise for advancing mechanism-driven studies.

This review presents a conceptual framework for AI-assisted mechanistic analysis in electrocatalysis. We focus on how AI can be integrated with operando experiments and atomistic simulations to address fundamental challenges in mechanism identification. Rather than cataloging AI applications, we position AI as a tool to transform complex operando data into interpretable representations and to expand the accessible scope of atomistic simulations (Fig. 1). Within this perspective, we examine representative electrocatalytic systems, including oxygen evolution reaction (OER), oxygen reduction reaction (ORR), and CO_2 reduction reaction (CO_2RR), to define the key mechanistic insights required for understanding catalytic function. We then assess how these insights are obtained through operando experiments and atomistic simulations, and where fundamental limitations arise in resolving dynamic states, interfacial effects, and reaction pathways. Building on this, we explore how AI can be integrated into these processes to extend mechanistic interpretation. Finally, we highlight recent developments and outline an emerging framework in which operando analysis and atomistic simulations are increasingly connected through AI, pointing toward a closed-loop approach to mechanistic studies.

2. Mechanistic challenges

Electrocatalytic systems such as OER, ORR, and CO_2RR involve distinct reactants and operating conditions yet share a common mechanistic foundation as surface-mediated reactions governed by transient intermediates [41–45]. Understanding these mechanisms is essential for establishing how catalytic structure, reaction environment, and

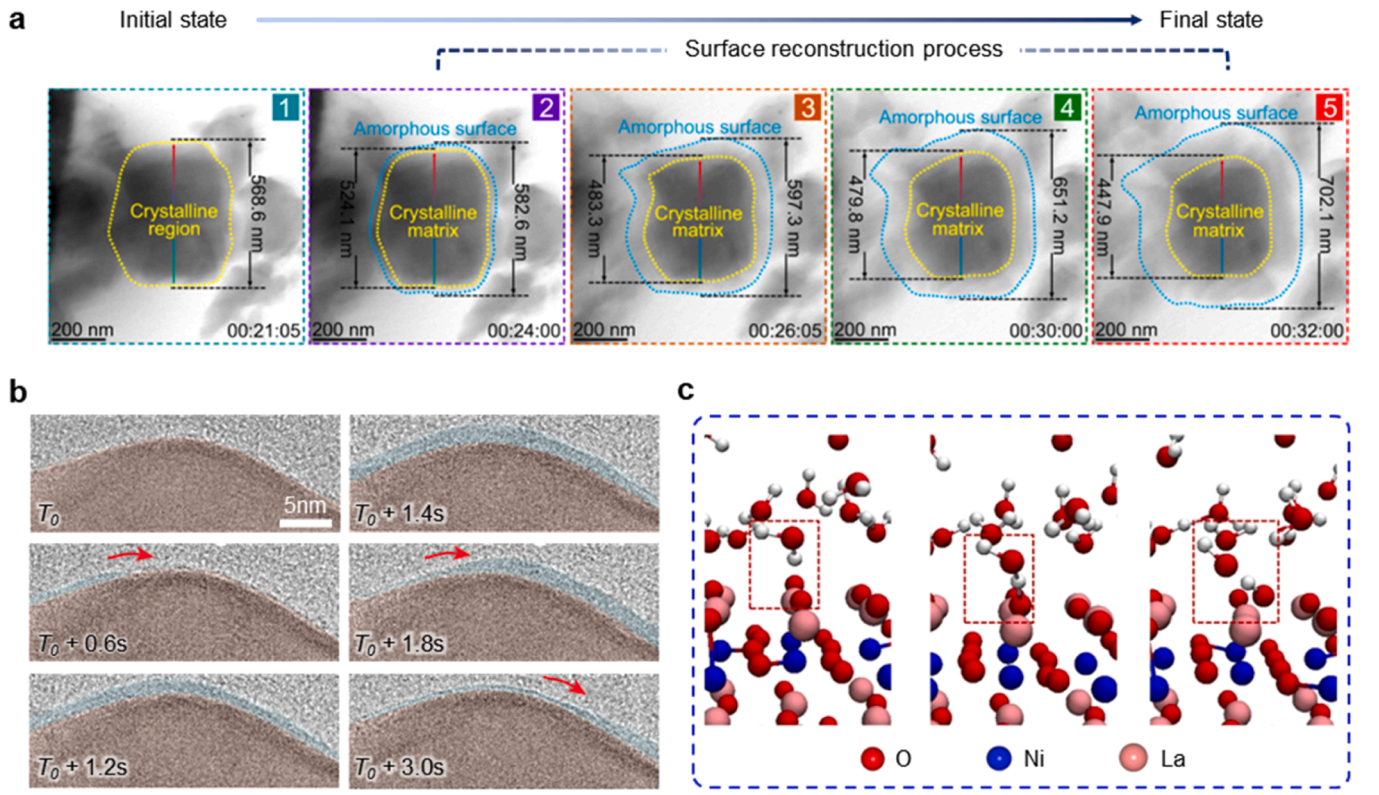

Fig. 2. a) Time-resolved operando TEM images showing the formation of an amorphous surface shell under the applied voltage of 0.9 V. Reproduced with permission from Ref. [57]. Copyright 2023 Springer Nature. b) Time-resolved HRTEM images of Cu surface showing lateral flow of the amorphous interphase. Reproduced with permission from Ref. [58]. Copyright 2024 Springer Nature. c) AIMD snapshots showing the spontaneous surface reconstruction of $LaNiO_3$ into an amorphous oxyhydroxide phase. Reproduced with permission from Ref. [40]. Copyright 2023 Wiley-VCH GmbH.

dynamic processes determine activity and selectivity, and thus for guiding rational catalyst design [46].

In this section, rather than comparing these systems individually, we focus on the common mechanistic challenges that arise across them, particularly in resolving catalytic states, their evolution under reaction environments, and their connection to reaction pathways and selectivity. These interconnected aspects define the key mechanistic insights required for understanding electrocatalytic function and, importantly, where current approaches encounter fundamental limitations.

2.1. State identification and evolution

Defining the identity of catalytic active states is a central objective in mechanistic studies of electrocatalysis. Under operating conditions, catalyst surfaces undergo continuous structural and electronic evolution in response to applied potential, adsorbate interactions, and interfacial processes [47–54]. As a result, catalytic states are represented by dynamically evolving configurations distributed across space and time, rather than by a single static structure [55].

Operando transmission electron microscopy (TEM) enables direct visualization of these structural transformations under electrochemical bias [56–60]. In oxygen evolution systems, electrochemical TEM (EC-TEM) studies of transition-metal sulfides reveal lattice-level transformations, including oxygen incorporation and sulfur depletion, which initiate surface reconstruction prior to steady-state catalysis (Fig. 2a) [57]. In CO_2RR systems, liquid-cell TEM (LC-TEM) measurements show that crystalline Cu surfaces evolve into amorphous, Cu-containing interphases that dynamically interconvert with the underlying lattice and exhibit lateral mobility (Fig. 2b) [58]. These observations unambiguously demonstrate the spatial and temporal evolution of catalytic structures under reaction conditions.

Atomistic simulations provide complementary insight into the mechanisms underlying this evolution. Constant-potential density functional theory (DFT) and ab initio molecular dynamics (AIMD) simulations capture how electrochemical bias and adsorbate interactions influence structural stability and drive transitions between configurations [40,53,61–63]. For example, in Cu–N–C single-atom catalysts, hydrogen adsorption modifies metal–ligand coordination and facilitates aggregation, while cooperative interactions between adsorbates promote the formation of mobile surface complexes [61]. In oxide catalysts, simulations reveal reconstruction processes driven by lattice oxygen activation and interfacial reactions, leading to the formation of oxyhydroxide-like phases under operating conditions (Fig. 2c) [40]. Together, these approaches unveil the structural evolution of catalytic states across highly dynamic systems.

2.2. Environment and interface effects

Catalytic states in electrocatalysis are defined by their interaction with the surrounding electrochemical environment. Applied potential, electrolyte composition, interfacial electric fields, and adsorbate interactions collectively determine the accessible structural, electronic, and chemical configurations of the catalyst [64–68]. As a result, catalytic behavior reflects the coupled evolution of catalyst and environment under operating conditions.

Operando X-ray absorption spectroscopy (XAS) enables direct access to probe the element-specific coordination and electronic structure in liquid electrolytes [54,69]. In transition-metal oxyhydroxide catalysts, X-ray absorption near edge structure (XANES) and extended X-ray absorption fine structure (EXAFS) measurements show that catalytic activation is associated with changes in local coordination geometry and metal–oxygen electronic structure under applied potential [70]. Variations in XAS features capture reversible symmetry changes and evolving metal–ligand interactions, providing insight into coordination-state

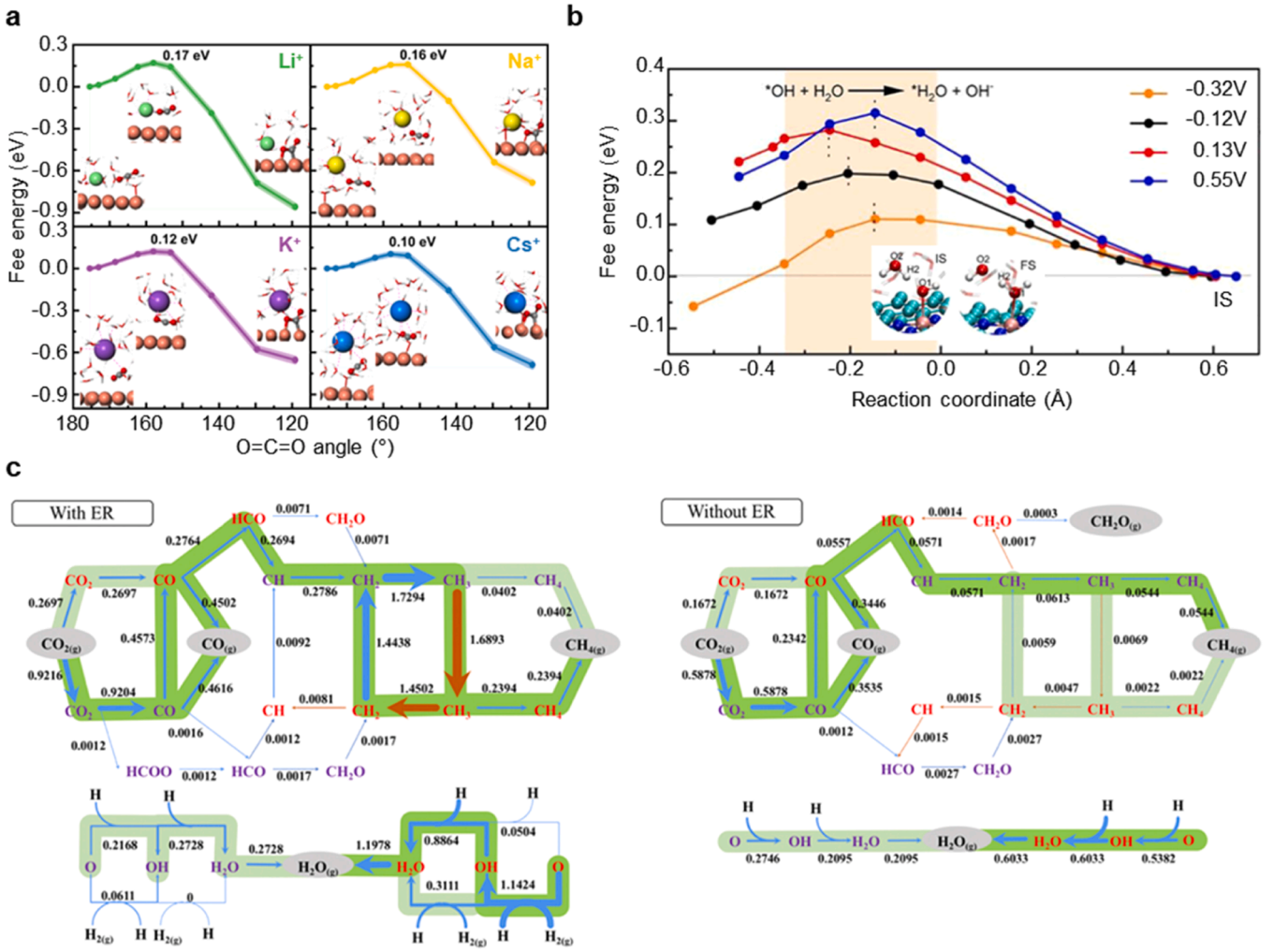

Fig. 3. a) AIMD simulations illustrating the critical role of alkali metal cations in modifying the CO_2 activation barrier through different coordination abilities of Li^+, Na^+, K^+, and Cs^+ on Cu(100) surfaces. Reproduced with permission from Ref. [80]. Copyright 2024 Springer Nature. b) Free energy profile for the ORR pathway on the Fe-N_4-C electrocatalyst, illustrating the thermodynamic energetics of the reaction steps. Reproduced with permission from Ref. [83]. Copyright 2023 American Chemical Society. c) Schematic representations of the executed reaction events derived from kMC simulations, illustrating the shift in dominant reaction pathways depending on the inclusion of Eley-Rideal (ER) reactions. Reproduced with permission from Ref. [87]. Copyright 2024 American Chemical Society.

evolution under electrochemical conditions [71].

Interfacial dynamics further define catalytic states through time-dependent interactions between the catalyst and surrounding species. Time-resolved operando measurements uncover progressive evolution of electronic states with applied potential and reaction time [72,73]. Vibrational techniques, such as Raman and infrared spectroscopies, resolve bond-specific signatures of surface adsorbates and reveal continuously evolving ensembles of species at the interface [74–79]. For example, in CO_2 reduction, operando surface-enhanced Raman spectroscopy (SERS) captures redistribution of adsorbates such as CO_{ad} and OH_{ad} under pulsed electrochemical conditions, revealing the nature of dynamic interfacial configurations [75].

Atomistic simulations yield further microscopic insights into these interactions by explicitly modeling the electrolyte environment [80–84]. Molecular dynamics (MD) and ab initio simulations show that solvent molecules, ions, and electric fields actively influence reaction energetics and intermediate stability. In CO_2 reduction on Cu surfaces, cation–adsorbate interactions modify activation barriers and adsorption configurations (Fig. 3a) [80], while in oxygen reduction systems, restructuring of interfacial water networks alters hydrogen-bond connectivity and reaction energetics (Fig. 3b) [83]. These approaches enable detailed investigation of catalyst–environment coupling and its influence on catalytic states.

2.3. Reaction pathway and selectivity

Mechanistic analysis of electrocatalysis requires identification of reaction pathways that connect catalytic states to product formation. In multistep electrochemical reactions, multiple reaction routes can proceed concurrently, and overall selectivity reflects the distribution of elementary steps occurring at the catalyst surface [45]. Understanding reaction mechanisms therefore involves resolving the formation, transformation, and consumption of intermediates along different pathways.

Atomistic simulations serve as a primary framework for mapping these reaction pathways. DFT calculations identify stable intermediate and elementary reaction steps, enabling construction of reaction networks that describe possible transformation routes [44,85].

Beyond static pathway identification, statistical simulation methods capture the dynamic selection of reaction routes under operating conditions. Kinetic Monte Carlo (kMC) simulations incorporate time-dependent event selection and surface coverage evolution, enabling direct evaluation of how reaction flux is distributed across competing pathways [45,86–88]. For example, kMC simulations of CO_2 hydrogenation on Ni/CeO_2 catalysts reveal that reaction flux is governed by cooperative interactions between distinct active sites, where removal of surface oxygen dynamically enables intermediate diffusion and completion of the catalytic cycle (Fig. 3c) [87]. These simulations

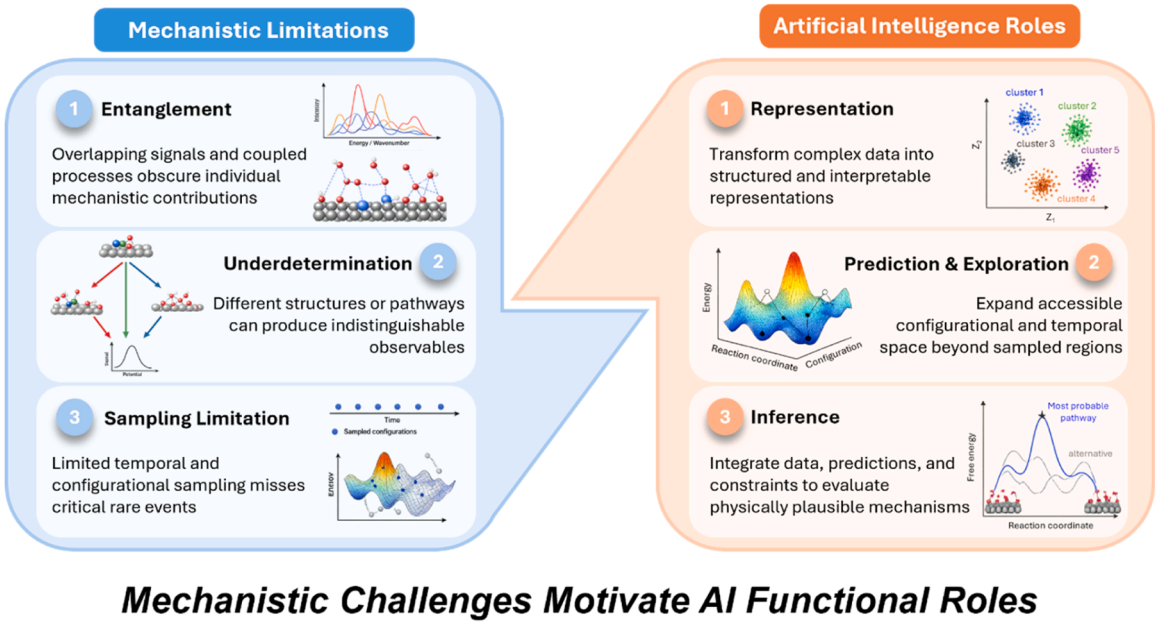

Fig. 4. Conceptual framework connecting mechanistic limitations in electrocatalysis with the functional roles of AI-derived analysis.

further show that different products emerge from distinct pathways within the same reaction network, such as CO formation via a reverse water–gas shift route and CH_4 formation through a formyl-mediated pathway.

Statistical approaches also reveal how reaction pathways evolve with applied potential and surface conditions. In CO_2 reduction on Cu surfaces, kMC simulations demonstrate that surface coverage transitions with increasing overpotential, leading to changes in dominant reaction routes and shifts in rate-determining steps. These results illustrate how pathway selection is dynamically regulated by reaction conditions through changes in reaction flux [88].

2.4. Challenges

The capabilities outlined in Sections 2.1–2.3 demonstrate that operando experiments and atomistic simulations provide access to catalytic states, their environment-dependent evolution, and associated reaction pathways. However, translating these observations into a definitive mechanistic description remains fundamentally unresolved.

A primary challenge arises from the **entanglement** of catalytic states and their environments. As described in Section 2.1, catalytic structures continuously evolve under reaction conditions and exist as transient populations rather than isolated configurations. At the same time, as shown in Section 2.2, these states are strongly coupled to the surrounding electrochemical environment, where adsorbates, solvent molecules, and electric fields continuously reshape the accessible configurational space. Because these structural and environmental degrees of freedom evolve simultaneously, experimentally observed signals represent superpositions of multiple coexisting states and interactions, rather than direct signatures of individual configurations [89–92].

This complexity leads directly to an **underdetermined** problem in mechanistic interpretation. As discussed in Section 2.3, multiple reaction routes can originate from shared intermediates [93,94], and pathway selection depends on dynamic competition between elementary steps [45]. Consequently, similar intermediate populations or energetic landscapes can correspond to different dominant pathways, depending on reaction conditions and surface states. This prevents a unique mapping between observed intermediates and the underlying reaction mechanism.

These intrinsic challenges are further amplified by **sampling limitations** in both experimental and computational approaches. Operando techniques provide time-resolved and environment-specific information, but measurements remain indirect and often integrate signals over spatial and temporal domains. Atomistic simulations offer detailed insight into local structures and reaction energetics yet remain restricted in their ability to sample the full configurational, temporal, and ensemble space relevant to catalytic systems [66,95–98]. As a result, experimental observations and simulation results each provide partial and complementary views of a much larger mechanistic landscape.

Taken together, mechanistic analysis in electrocatalysis requires reconstructing relationships between evolving states, coupled environments, and competing pathways from incomplete and indirect observations. These challenges can be understood in terms of three interrelated limitations: entanglement, underdetermination, and sampling limitations. This establishes the need for analytical frameworks capable of integrating heterogeneous data, disentangling coupled variables, and extracting mechanistic information from complex datasets.

3. AI Framework

Building on the fundamental challenges identified in Section 2, this section establishes a role-based framework for integrating AI into mechanistic analysis. Rather than treating AI as a collection of individual models, the framework organizes its contribution according to the mechanistic problems it addresses, the methods through which it can be implemented, and the reliability criteria required for meaningful interpretation. This structure provides the basis for defining the functional roles of AI, mapping them to representative methodological approaches, and evaluating their limitations and physical consistency.

3.1. Roles in mechanistic analysis

The limitations summarized in Section 2.4 highlight three major requirements for AI-assisted mechanistic analysis: organizing incomplete and convoluted data, expanding the accessible state space, and supporting physically meaningful interpretation. Accordingly, AI can be understood in terms of three functional roles: representation, prediction and exploration, and inference (Fig. 4). These roles are not independent categories, but interconnected steps that link data transformation, state-

Table 1
Representative AI methods and their functional roles in mechanistic analysis.

AI role	AI approach	Method / Model type	Function	Role in mechanistic analysis	Typical application	Ref.
Representation	Deep learning	Autoencoder (AE), CNN	Nonlinear feature extraction	Extraction of latent features associated with catalytic states from complex operando signals	Spectroscopic pattern recognition (XAS, Raman)	[99, 100]
	Unsupervised / self-supervised learning	Deep clustering, contrastive learning	Representation learning without labels	Grouping of similar spectral or structural patterns and temporal evolution	Time-resolved operando data analysis	[101]
Prediction & exploration	ML interatomic potentials	Deep MD	Scalable energy and force prediction	Atomistic simulations under realistic electrochemical environments	Electrochemical interface modeling	[102]
		Neural Network Potentials (NNP), HDNNP	Energy and force prediction	Exploration of large configurational space beyond DFT limits	Large-scale MD simulations of catalytic surfaces	[103]
	Graph neural networks	SchNet, DimeNet, ALIGNN	Structure-property mapping	Prediction of adsorption energies and structure-property relationships	Catalyst surface and material modeling	[104, 105]
	Active learning framework	Adaptive sampling (ANI, DP-GEN)	Iterative model refinement	Efficient exploration of configurational space and rare events	Accelerated simulation workflows	[106]
Inference	Probabilistic models	Bayesian inference	Uncertainty-aware modeling	Probabilistic assessment of competing mechanistic hypotheses	Reaction network analysis	[107]
	Generative models	Variational Autoencoder (VAE)	Latent space sampling and data generation	Generation of plausible reaction configurations or pathways	Mechanism exploration and inverse design	[108]
		Diffusion models	Probabilistic generation	Sampling of plausible structure or reaction configurations	Molecular and reaction pathway generation	[109]
	Learning-based optimization	Reinforcement learning (RL)	Policy optimization	Optimization of reaction sequences or catalytic design strategies	Catalyst design and mechanism search	[110, 111]

space expansion, and mechanistic interpretation.

The first role, **representation**, converts complex and noisy data into structured descriptors that capture underlying catalytic states. In operando analysis, this involves extracting latent features from overlapping spectroscopic signals or time-resolved measurements, thereby enabling patterns to be identified beyond direct observability. This step defines how information is encoded and directly constrains the scope of subsequent analysis.

The second role, **prediction and exploration**, extends these representations into a broader configurational and energetic space. By learning structure–property relationships, AI models enable efficient sampling of atomic configurations, reaction intermediates, and dynamic surface states that are otherwise inaccessible through conventional simulations. This role bridges experimentally observed signals with the underlying atomistic landscape.

The third role, **inference**, connects the explored state space to mechanistic interpretation. Rather than providing definitive solutions, AI-based inference evaluates competing hypotheses and identifies physically plausible reaction pathways based on available data and learned relationships. This process inherently involves uncertainty and requires consistency with physical principles to ensure meaningful interpretation.

Taken together, these roles define a hierarchical workflow in which representation establishes the information space, prediction and exploration expand it, and inference assigns mechanistic meaning. Mechanistic understanding therefore emerges from the integration of these functions, rather than from any single model or method.

3.2. Methods and implementation

While the roles defined in Section 3.1 describe the functional structure of AI-assisted mechanistic analysis, their practical realization depends on the selection and integration of appropriate computational methods. Different roles require distinct data processing, modeling, and interpretation strategies, depending on the nature of the data input, the scale of the system, and the level of mechanistic detail required.

Rather than reviewing individual models in isolation, we organize representative AI approaches according to their functional roles in mechanistic analysis, as summarized in Table 1. This role-based classification provides a structured mapping between AI methods and their contributions to data representation, state-space exploration, and mechanistic inference. It also facilitates comparison between different approaches and clarifies their applicability across operando analysis and atomistic simulations.

Importantly, these roles are not uniquely associated with specific models, as the same method can be adapted to perform different functions depending on the task. This flexibility enables the integration of multiple approaches within a unified workflow, rather than restricting analysis to fixed model categories. The framework presented here therefore emphasizes functional relationships over model types, providing a flexible basis for applying AI in mechanistic studies.

Table 2
Reliability, and evaluation of AI-assisted mechanistic analysis.

AI Challenge	Origin	Impact on mechanistic interpretation	Current strategies
Data quality and noise	Noisy, overlapping, and time-resolved operando spectroscopic signals with limited direct structural observability	Ambiguous identification of transient catalytic states and reaction intermediates under dynamic electrochemical conditions	Advanced signal processing, data denoising, and multimodal data integration
Model interpretability	Limited physical interpretability of learned features in deep learning models applied to spectroscopic and atomistic data	Difficulty in linking extracted features to physically meaningful reaction coordinates and catalytic mechanisms	Explainable AI (XAI) and physically informed feature attribution methods
Generalization and transferability	Strong dependence on system-specific training data and sensitivity to changes in electrolyte, potential, and surface structure	Limited transferability of learned models across different electrochemical and catalyst surfaces	Domain adaptation and cross-condition transfer learning
Physical inconsistency	Absence of explicit thermodynamic, kinetic, and electrochemical constraints in purely data-driven models	Generation of energetically or kinetically inconsistent reaction pathways and misleading mechanistic interpretations	Physics-informed models and hybrid simulation-AI framework

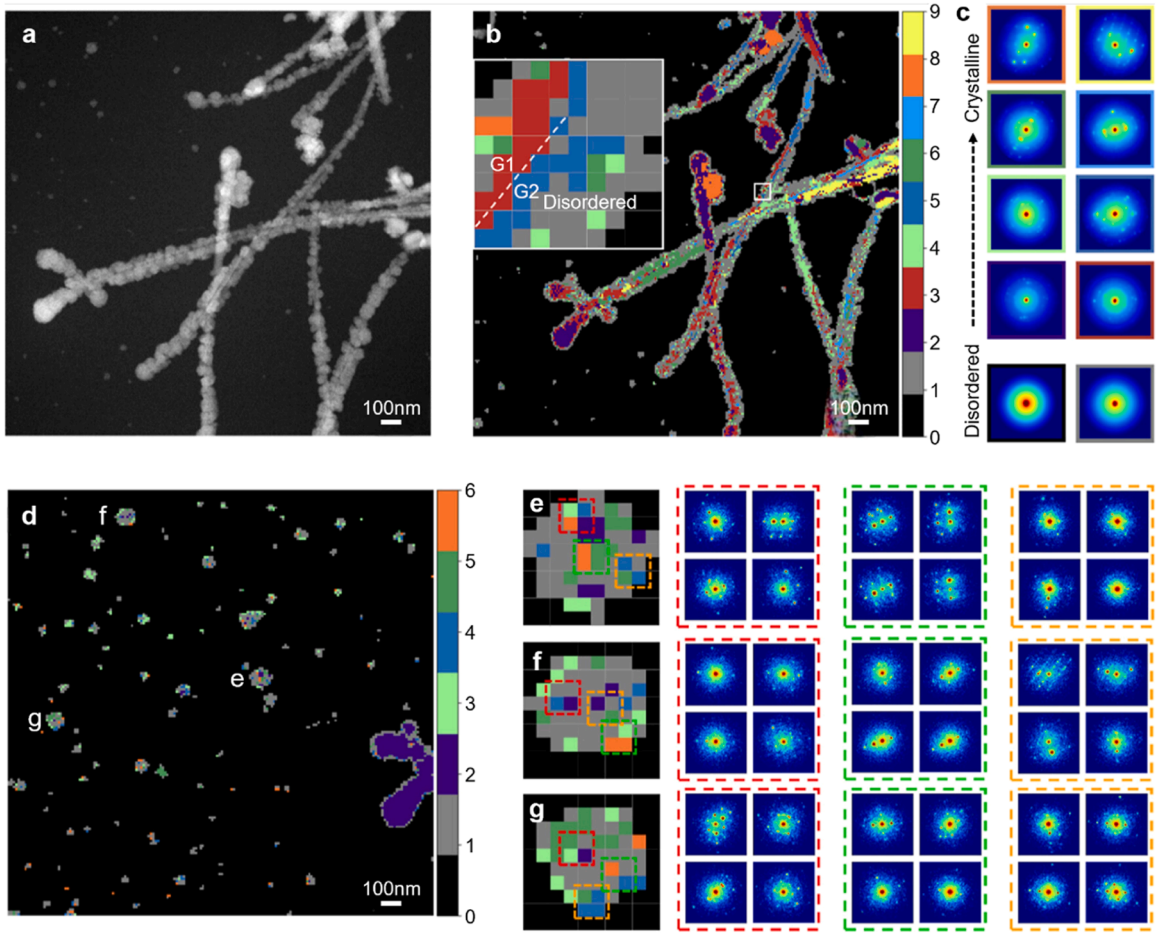

Fig. 5. a) Operando HAADF-STEM image and b) the corresponding 4D-STEM clustering map of a Cu nanowire, distinguishing the crystalline core from the disordered spongy shell. c) Representative electron diffraction patterns extracted from the clustering analysis. d) Operando 4D-STEM clustering map of the nanowire-derived polycrystalline Cu nanograins. e-g) Detailed clustering maps and corresponding diffraction patterns of selected individual nanograins from d), resolving distinct crystallographic orientations across grain boundaries. Reproduced with permission from Ref. [132]. Copyright 2024 American Chemical Society.

3.3. Reliability and physical consistency

The integration of AI into mechanistic analysis introduces challenges that are distinct from those encountered in conventional data analysis or simulation. While AI enables the extraction and exploration of complex relationships, it does not inherently guarantee that the resulting interpretations are physically meaningful or mechanistically reliable [112, 113]. As a result, the use of AI requires careful consideration of the conditions under which its output can be interpreted with confidence.

These challenges can be broadly categorized into four interrelated aspects, as summarized in Table 2: data quality and noise, model interpretability, generalization and transferability, and physical consistency. Each of these factors directly affects the reliability of mechanistic interpretation. Noisy or indirect operando signals can lead to ambiguous representations of catalytic states, while limited or biased datasets constrain model generalization across different reaction conditions [114–117]. At the same time, the black-box nature of many AI models obscures the relationship between input features and predicted outcomes, making it difficult to establish causal links [118–120]. Furthermore, the absence of explicit physical constraints may result in predictions that are inconsistent with thermodynamic or kinetic principles [112,121–123].

Importantly, these challenges do not arise independently but are strongly coupled within the mechanistic analysis workflow. Limitations in data quality propagate through representation and prediction steps, while poor interpretability and lack of physical consistency can compromise inference. Consequently, the reliability of AI-assisted mechanistic analysis depends not only on model performance, but on the consistent integration of data quality, interpretability, and physical constraints. Addressing these factors is therefore essential for ensuring that AI contributes to mechanistic understanding rather than merely generating plausible but unverified interpretations.

4. Applications in mechanistic analysis

The framework introduced in Section 3 defines the functional roles of AI in mechanistic analysis, including representation, prediction and exploration, and inference. In practice, however, these roles are not implemented in isolation but are realized through diverse analytical workflows that combine different types of data processing and modeling approaches. As a result, the contribution of AI often emerges as part of an integrated analysis pipeline rather than as a standalone component.

In this section, we examine how these functional roles are reflected in current mechanistic studies, with a focus on their implementation in operando analysis and atomistic simulations. In practice, many key analytical steps are still predominantly performed using statistical and data-driven approaches that structure complex datasets into interpretable components. Therefore, rather than restricting the discussion to fully AI-driven implementations, we consider how different analytical strategies contribute to mechanistic interpretation. This perspective reflects the evolving nature of the field, in which AI is progressively integrated into existing workflows to enhance the interpretation of

complex experimental and computational data.

4.1. AI-integrated operando analysis

Operando electrocatalytic measurements, as discussed in Section 2, produce complex signals arising from dynamically evolving and coexisting catalytic states, which inherently limit direct mechanistic interpretation. Within the framework defined in Section 3, these challenges can be understood in terms of representation and inference, where experimental observables must be transformed into meaningful state descriptors and linked to mechanistic interpretation.

In practice, this transformation is not achieved in a single step, but through a sequence of analytical processes, including data qualification, state separation, and structure extraction. These steps are not independent, but are sequentially connected within a unified workflow, where the output of each stage defines the input of the next. Within this framework, AI-based and data-driven methods operate across multiple stages, enabling the systematic transition from raw operando measurements to mechanistically interpretable descriptors [124,125].

4.1.1. Data qualification

Within AI-assisted operando analysis workflow, data qualification represents a distinct and foundational analytical step. Rather than directly extracting mechanistic descriptors, data qualification aims to assess whether operando datasets are internally consistent, statistically robust, and suitable for downstream state separation or structural interpretation [126]. In this framework, machine learning (ML) can be employed to evaluate signal stability, discriminate artefact-dominated regions, and define analyzable signal domains prior to mechanistic analysis. For example, Yao *et al.* utilized ML-based segmentation not as a means of inferring particle dynamics per se, but to establish reliable particle boundaries in noise-dominated liquid-phase transmission electron microscopy (LP-TEM) videos, thereby defining which portions of the dataset could be meaningfully analyzed [127]. Likewise, Sun *et al.* applied deep-learning models to isolate physically meaningful nanoparticle features from fluctuating operando backgrounds, enabling subsequent quantitative analysis only after artefact-prone regions had been excluded [128].

The role of ML-assisted data qualification becomes even more critical for high-dimensional operando datasets, such as four- and five-dimensional scanning transmission electron microscopy (4D/5D-STEM). Lee *et al.* explicitly addressed this challenge by demonstrating that operando diffraction datasets acquired in liquid-cell environments contain substantial fractions of low-information or noise-dominated diffraction patterns that compromise unsupervised clustering analysis [129]. By implementing background masking and similarity-based

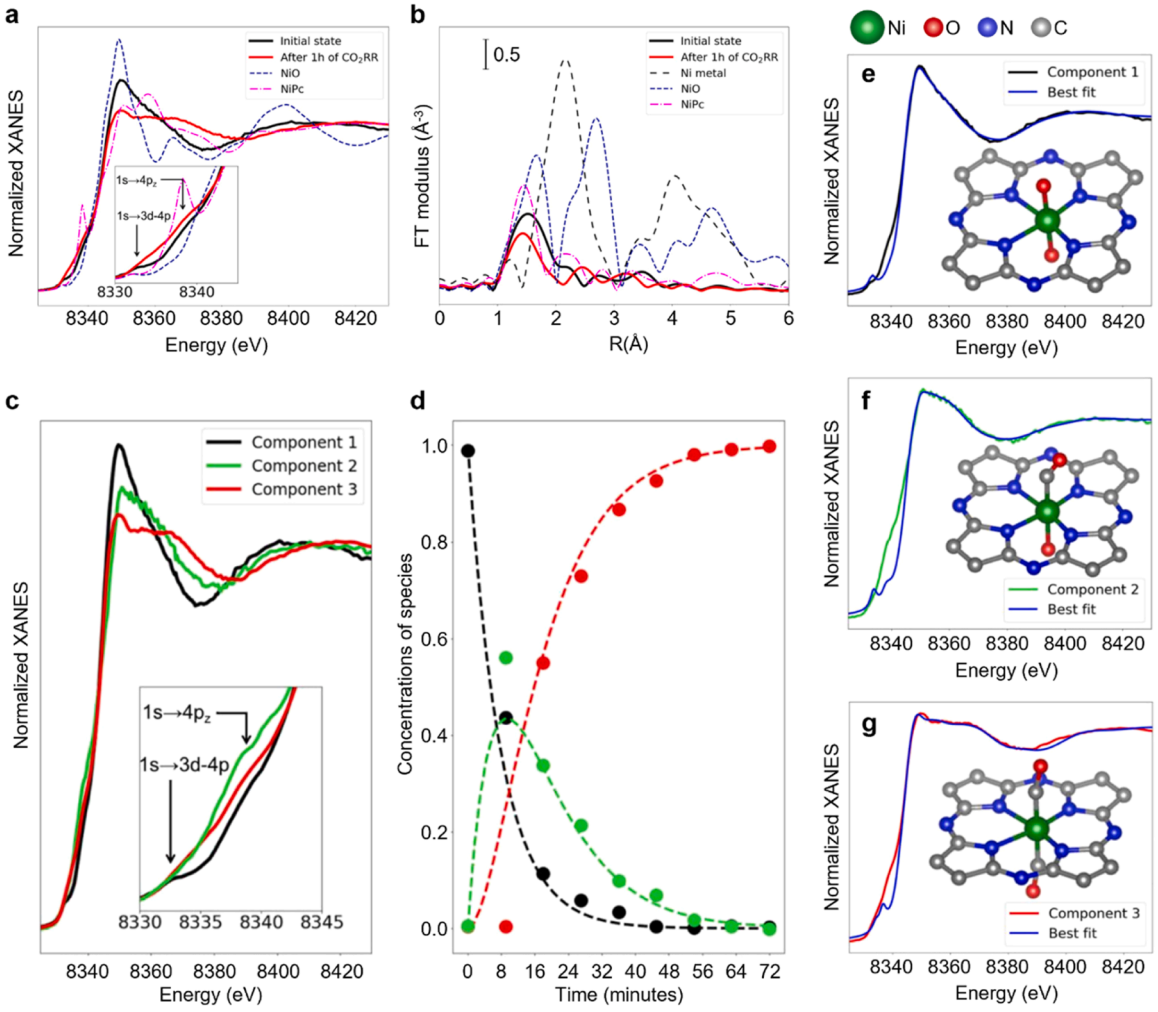

Fig. 6. Operando Ni K-edge a) XANES and b) magnitudes of the FT-EXAFS (phase uncorrected) spectra collected before and at the end of the CO_2RR (after 1 h) for the HT Ni-TMNC sample. c) XANES spectra for the extracted pure species and d) related concentration profiles (filled circles) extracted via TM approach from the experimental Ni K-edge XANES data for the HT Ni-TMNC sample. e-g) Comparison of the XANES components for pure species, as extracted from the experimental data, with the best-fit results. Insets show the final structure models obtained in the XANES fitting. Reproduced with permission from Ref. [138]. Copyright 2023 American Chemical Society.

validation prior to clustering, they established a qualified subset of diffraction data that could be reliably subjected to downstream state separation. Similarly, the framework introduced by Wang *et al.* employed unsupervised ML to define statistically reliable nanoparticle populations in TEM datasets, explicitly framing ML as a tool for determining what constitutes valid data before any structural or kinetic interpretation is attempted [130].

These studies underscore that ML-based data qualification is conceptually distinct from state separation or structural inference. As emphasized by Scott *et al.*, unsupervised analysis of large 4D-STEM datasets is highly sensitive to feature representation and preprocessing choices, and clustering results can vary substantially in the absence of robust qualification strategies [131]. Together, these findings illustrate that data qualification is not an optional preprocessing step, but a prerequisite for reliable AI-assisted operando analysis. By establishing which portions of complex operando datasets are physically meaningful and statistically consistent, data qualification provides the necessary foundation upon which subsequent state separation and structure extraction can be performed with confidence.

The relevance of data qualification becomes particularly evident in operando electrocatalytic systems, where catalyst restructuring, gas evolution, and electrochemical reactions proceed simultaneously under highly dynamic and noise-prone conditions [133,134]. Yang *et al.* employed operando electrochemical 4D-STEM combined with ML–assisted data qualification to investigate Cu nanowire–derived catalysts under CO_2 reduction conditions (Fig. 5) [132]. In operando 4D-STEM, a full electron diffraction pattern is recorded at each probe position, generating an exceptionally high-dimensional dataset that is highly susceptible to noise, beam-induced damage, and structural disorder.

Rather than directly interpreting individual diffraction patterns, Yang *et al.* applied unsupervised clustering as a data qualification strategy to identify statistically consistent diffraction signatures across the dataset [132]. As shown in the false-color clustering maps (Fig. 5a, b), this approach enabled discrimination between the crystalline Cu nanowire core and a surrounding spongy, disordered Cu shell, while simultaneously excluding low-information or artefact-dominated diffraction patterns. This clustering-based analysis served to validate which portions of the operando 4D-STEM dataset were physically meaningful, rather than to infer catalytic states directly.

Following this qualification step, the authors analyzed selected polycrystalline Cu nanograins formed during electrochemical operation (Fig. 5d), demonstrating that crystallographic orientations across grain boundaries could be resolved without imposing prior assumptions regarding phase purity or structural uniformity (Fig. 5e–g) [132]. In this framework, ML-based analysis serves as a gatekeeping step that establishes data reliability prior to interpretation, thereby preventing misassignment of transient or artefact-induced features as catalytically relevant structures. This study illustrates how data qualification transforms raw, noise-prone operando 4D-STEM measurements into analytically trustworthy representations, providing a necessary foundation for subsequent state separation and structure extraction in operando electrocatalysis.

4.1.2. Data separation

Following data qualification, a critical analytical task in operando electrocatalysis is the resolution of coexisting catalytic states embedded within ensemble-averaged measurements. To address this challenge, data-driven statistical decomposition methods are employed to separate mixed operando datasets into distinct components prior to mechanistic interpretation. These approaches aim to extract statistically independent spectral or structural contributions without relying on predefined reference states, thereby providing an intermediate representation of the system that can guide subsequent analysis.

To date, data separation in operando analysis has been predominantly performed using data-driven statistical decomposition methods, which aim to resolve mixed signals into statistically independent components. Voronov *et al.* demonstrated that multivariate curve resolution (MCR) can function as a blind-source separation strategy for in situ and operando XAS, enabling extraction of pure spectral components and their associated concentration profiles without relying on predefined reference compounds [135]. In a related approach, Cassinelli *et al.* applied principal component analysis (PCA) followed by constrained matrix factorization to time-resolved XAS measurements, revealing the presence of multiple transient species that could be resolved through conventional linear combination fitting [136]. More importantly, Martini *et al.* emphasized that successful spectral decomposition must satisfy both mathematical consistency and physico-chemical plausibility, underscoring that statistical separation alone does not establish mechanistic identity [137].

Extending these methodological principles to operando electrocatalysis, Martini *et al.* further addressed transformation-mixed-based separation to time-resolved Ni K-edge XANES spectra acquired during CO_2 reduction on Ni-TMNC catalysts (Fig. 6) [138]. The measured spectra exhibited continuous evolution arising from multiple coexisting Ni coordination environments. To resolve these contributions, PCA was first applied to determine the number of statistically significant components required to describe the dataset. PCA identified multiple independent spectral contributors beyond those accessible through direct linear combination fitting [138].

Based on this dimensionality analysis, a transformative-matrix (TM) approach was implemented to extract pure component spectrum and their corresponding concentration profiles from the mixed operando dataset [138]. As shown in Fig. 6c, the extracted XANES components correspond to spectroscopically distinct Ni species. These species cannot be isolated experimentally but are resolved through data-driven decomposition. The associated concentration profiles (Fig. 6d) quantify the dynamic interconversion of these species during electrochemical operation. The extracted spectral components were subsequently subjected to XANES fitting to determine coordination geometries and structural models (Fig. 6e-g), establishing a direct pathway from statistically separated spectral states to atomically defined Ni environments, which is discussed in the following subsection.

Conceptually, data separation occupies an intermediate position within the data-driven operando analysis framework. Whereas data qualification ensures that measurements are physically reliable, data separation resolves the internal heterogeneity of qualified datasets by identifying coexisting states. The resulting components are statistically defined and model-agnostic, providing structured representations that guide, but do not replace subsequent structural interpretation.

4.1.3. Structure extraction and inference

While data separation isolates spectroscopically independent components, these signatures remain without assigned atomic structure until explicitly mapped onto atomic configurations. The transition from spectral signatures to atomic identity therefore constitutes a fundamentally inverse problem in operando analysis, requiring a quantitative relationship between measured observables and underlying structural parameters [139].

In conventional operando XAS analysis, structural interpretation relies on predefined structural models and limited parameter fitting within constrained coordination shells. Such approaches become increasingly inadequate under working conditions, including non-ideal distortions, symmetry breaking, alloying, or phase interconversion. Data-driven structure extraction extends beyond reference-based fitting by enabling high-dimensional exploration of structural parameter space and capturing nonlinear relationships between spectral features and atomic configurations [91,140]. Importantly, this process does not merely refine fitting accuracy; it reformulates spectral interpretation as a data-driven mapping from measurement to structural space.

In atomically dispersed catalysts, structural evolution under electrochemical bias is generally manifested as continuous geometric

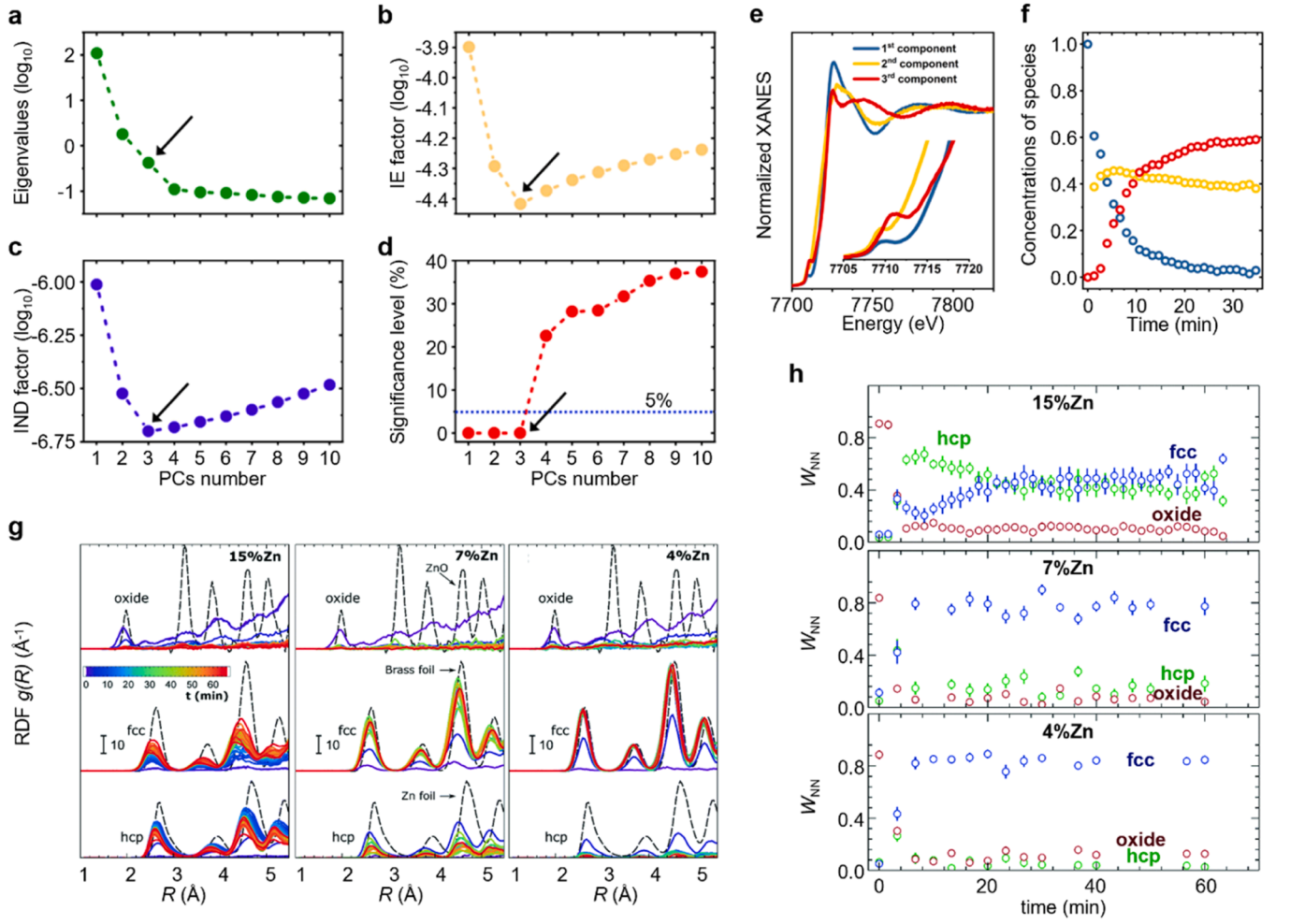

Fig. 7. a) Scree plot. b) Imbedded error plot. c) Malinowski indicator factor plot. d) Significance level plot derived from the Fisher test. The arrows point to the number of pure species contributing to the XANES dataset, as obtained from each test. For all of them, this number was found to correspond to 3. Pure XANES spectra e) and concentration profiles f) extracted by the TM approach. The inset in (e) shows a magnification of the pre-edge region for the three XANES components. Reproduced with permission from Ref. [141]. Copyright 2024 John Wiley and Sons. g) Time-dependent evolution of radial distribution functions obtained by the NN-EXAFS analysis from operando Zn K-edge EXAFS data for bimetallic catalysts with 15%, 7% and 4% Zn content. h) Evolution of the relative concentrations of oxide, fcc-like and hcp-like phases, as obtained by the NN from operando Zn K-edge EXAFS data for bimetallic catalysts with a Zn loading of 15%, 7% and 4% during CO_2RR at a current density of −500 mA cm^{-2}. Reproduced with permission from Ref. [142]. Copyright 2022 The Royal Society of Chemistry.

distortion while maintaining the coordination framework [141]. In this regime, structure extraction can be formulated within a continuous structural parameter space. As illustrated in Fig. 7a–g, Martini *et al.* employed PCA and complementary statistical criteria to establish the intrinsic dimensionality of the operando Co K-edge XANES dataset [141]. Scree plots, embedded error analysis, Malinowski indicators, and Fisher significance testing consistently indicated three independent spectral contributions (Fig. 7a–d). Transformation-matrix analysis then reconstructed the corresponding pure XANES spectra and their concentration profiles (Fig. 7f, g), thereby completing the separation stage.

To assign structural identity to these components, the spectra were interpreted within a simulated structural space covering diverse coordination geometries [141]. By establishing a quantitative mapping between spectral features and structural parameters, the analysis enabled continuous inversion of experimental spectra to extract bond distances, coordination asymmetry, and adsorbate-induced distortions under operando conditions. Structural evolution was thus expressed through continuously varying geometric descriptors rather than discrete reference compounds, extending operando spectroscopy from state discrimination to quantitative active-site geometry reconstruction [141].

In contrast, heterogeneous alloy catalysts exhibit structural evolution that reflects redistribution among coexisting structural domains rather than distortion of a single coordination motif [142]. For such systems, structure extraction must operate within a discrete motif space. This distinction is reflected in Fig. 7h, i, where Rüscher *et al.* analyzed operando Zn K-edge EXAFS data from Cu–Zn nanocatalysts during CO_2 reduction. Instead of parameterizing local bond distortions, theoretical datasets representing oxide, face-centered cubic (FCC)-like alloy, and hexagonal close-pack (HCP)-like alloy motifs were used to relate EXAFS oscillations to radial distribution functions [142]. As shown in Fig. 7h, time-dependent radial distribution functions were reconstructed directly from operando spectra, resolving changes in interatomic distances and coordination environments. Concurrently, the relative concentrations of oxide, fcc-like, and hcp-like phases were quantified as a function of reaction time (Fig. 7i), providing a dynamic description of alloying and phase interconversion under high current density.

In this motif-resolved framework, structural evolution is represented as redistribution among discrete structural ensembles rather than incremental bond distortion. Together, Fig. 7 illustrate two complementary formulations of structure extraction in operando electrocatalysis: continuous geometric inference within a single-site scaffold and motif-resolved reconstruction in heterogeneous systems. Despite methodological differences, both approaches translate statistically resolved operando spectra into explicit atomic-level descriptors that can be

Table 3
Analytical method for mechanistic interpretation in operando electrocatalytic analysis.

	Operando Technique	Reaction	Analytical Objective	Method	Representative Methods	Key Observation	Mechanistic Insight Enabled	Ref.
Data qualification	Operando 4D-STEM	CO_2RR	Diffraction-pattern clustering; spatial segmentation	Statistical / clustering	K-means–based hierarchical clustering; fluctuation electron microscopy	Coexistence of crystalline Cu nanograins, disordered regions, and heterogeneous grain boundaries under reaction conditions	Identification of polycrystalline Cu nanograin networks and grain boundaries as operando active structures, inaccessible by ensemble-averaged imaging	[132]
Data separation	Operando XANES	CO_2RR	Decomposition of mixed spectral signals; species number identification	Statistical decomposition	PCA; transformation matrix (TM) analysis	Extraction of three distinct Ni species with independent kinetic profiles during CO_2RR	Direct evidence for dynamic coexistence and interconversion of multiple single-atom Ni states under operating conditions	[138]
Structure extraction	Operando XANES	OER / ORR	Peak separation and structural motif inference from operando spectra	Hybrid (statistical + model-based)	PCA-assisted peak separation; ML-assisted spectral fitting	Resolution of overlapping oxidation-state and coordination motifs hidden in ensemble spectra	Reconstruction of transient active-site geometries and oxidation-state evolution during electrochemical reactions	[141]
	Operando XAS	CO_2RR	Mapping spectral features to local structural parameters	Machine learning / model-based	ML-based XANES fitting (RBF regression); adaptive sampling; Reverse Monte Carlo (RMC) validation	Quantitative determination of Ni–N, Ni–O, and Ni–CO bond distances and geometrical distortions	Atomistic identification of reaction-induced coordination changes and adsorbate binding in single-atom Ni sites	[142]

directly linked to catalytic mechanisms. In this context, AI-based approaches serve as an enabling framework for establishing relationships between experimental observables and atomic-level descriptors, complementing statistical decomposition and model-based analysis rather than replacing them [86].

Despite these advances, AI-assisted operando analysis remains subject to important conceptual and practical limitations. The inversion from spectral observables to atomic structure is fundamentally non-unique, and statistically separated components do not inherently guarantee physical identity [143]. Distinct coordination distortions, dynamic disorder, or adsorbate configurations may generate spectrally similar signatures, rendering structure extraction an ill-posed problem without additional physical constraints [144]. Moreover, supervised models depend strongly on the representativeness of training datasets, which are often derived from idealized simulations that may not fully capture realistic electrochemical complexity [145]. Even unsupervised decomposition methods such as PCA or MCR can yield different solutions depending on preprocessing choices and feature representation [146]. These considerations underscore that AI functions not as an autonomous interpreter, but as a statistically guided inference layer whose reliability depends on physically informed constraints, cross-validation with complementary techniques, and careful integration with mechanistic reasoning [144]

Across all stages of operando analysis, the use of AI does not eliminate uncertainty or guarantee correctness. Instead, it shifts the analytical process from subjective interpretation toward statistically defined and reproducible frameworks. While both manual and ML-based approaches remain sensitive to feature representation and preprocessing choices, AI-based methods enable systematic evaluation across large datasets, reducing operator-dependent bias and improving consistency.

Importantly, the reliability of AI-assisted analysis depends on validation strategies, including consistency across multiple representations, agreement with physically meaningful structures, and cross-verification with independent experimental or computational results. In this context, AI does not replace human judgment, but provides a structured and scalable framework for supporting mechanistic interpretation under complex operando conditions. These considerations highlight the need for physically consistent and generalizable modeling frameworks, which are discussed in Section 3.3 (Table 3).

4.2. AI-enabled molecular simulations

Atomistic simulations, as discussed in Section 2, provide a mechanistic link between atomic-scale energetics and electrocatalytic behavior, but are inherently limited in accessing the full configurational, temporal, and thermodynamic space of catalytic systems. Within the framework defined in Section 3, these limitations primarily constrain prediction and exploration, where mechanistic understanding depends on the extent of accessible state space.

AI-based approaches address this limitation by enabling systematic expansion of the accessible simulation domain. Machine-learning interatomic potentials (MLPs) extend atomistic simulations to larger length and time scales while retaining near first-principles accuracy, thereby overcoming key bottlenecks in conventional approaches [147, 148]. As illustrated in Fig. 8a, MLP-based simulations extend the accessible time–length domain beyond the intrinsic limits of ab initio methods. More broadly, the impact of AI on molecular simulation can be understood as an expansion across three interrelated dimensions—configurational, temporal, and ensemble space [151]. This shift enables mechanistic analysis to move beyond isolated configurations toward statistically meaningful descriptions of dynamically evolving catalytic systems.

Importantly, this expansion is not achieved through purely data-driven fitting but is grounded in physically consistent modeling frameworks as mentioned in Section 3.3. Machine-learning interatomic potentials are trained on first-principles reference data and preserve key

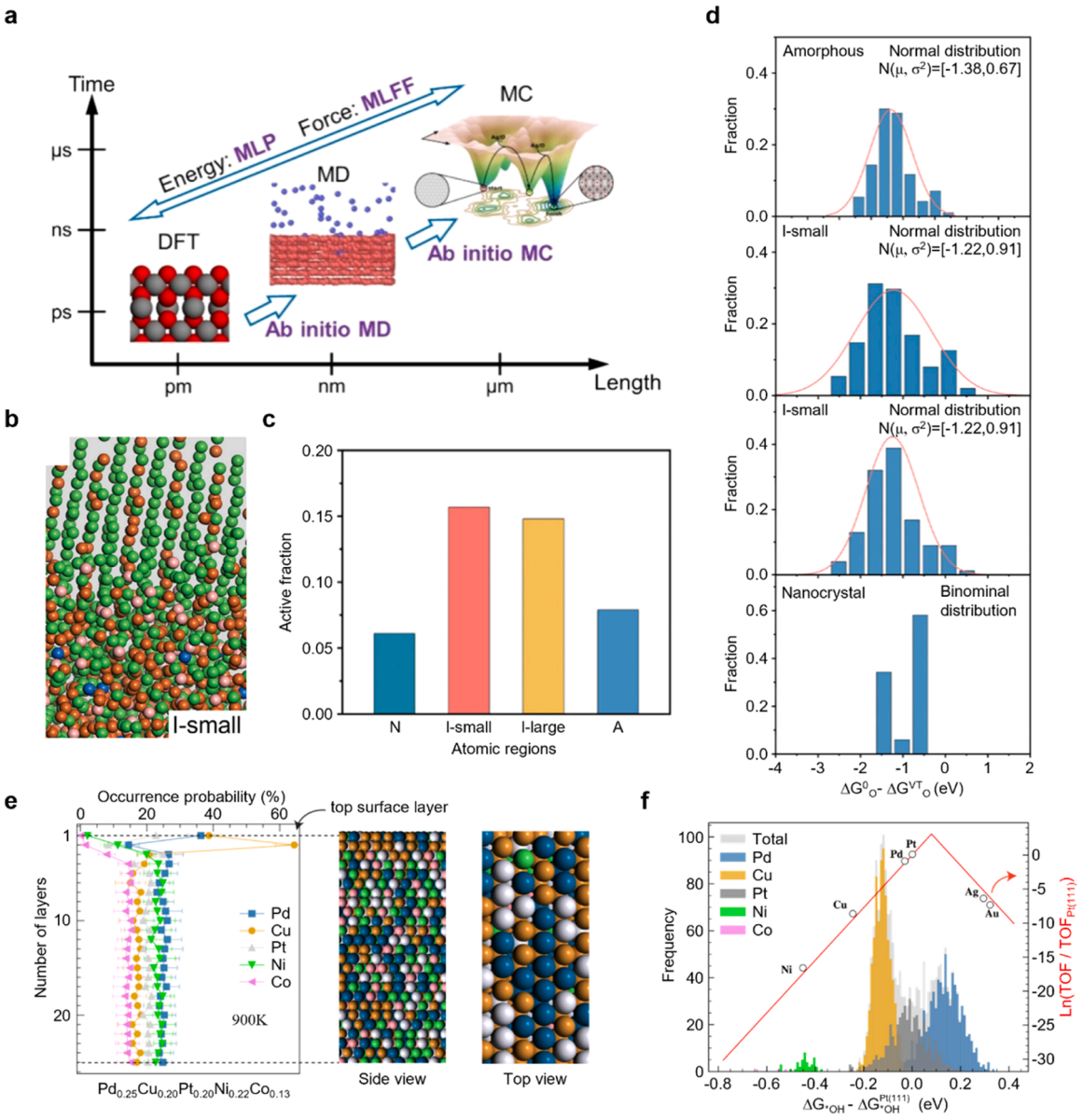

Fig. 8. a) Schematic overview of operando computational methods bridging different length- and time-scales in combination with ML. Reproduced with permission from Ref. [98]. Copyright 2023 John Wiley and Sons. b) Atomic models of N/A alloy interfaces optimized via HDNNP-based annealing simulations for large-scale configurational sampling. c) Fractions of active sites across different atomic regions within the sampled N/A interfaces. Reproduced with permission from Ref. [149]. Copyright 2024 John Wiley and Sons. d) Statistical distributions of the OER adsorption energy descriptor derived from the HDNNP sampling, demonstrating that structural heterogeneity broadens the dispersion and increases the probability of generating near-optimal sites. e) Thermodynamically equilibrated surface segregation profiles of a PdCuPtNiCo HEA, obtained through large-scale sampling using ALIGNN and MC simulations. f) ML-predicted OH adsorption free energy histograms and the ORR activity map of the HEA surface, showing that compositional segregation shifts the energy distribution and increases the statistical population of near-optimal sites. Reproduced with permission from Ref. [150]. Copyright 2024 American Chemical Society.

physical properties, such as energy conservation, symmetry invariance, and force consistency. As a result, the expanded sampling enabled by AI remains anchored to physically meaningful potential energy surfaces, extending the applicability of atomistic simulations without compromising physical fidelity. Together, these developments establish a framework in which configurational, temporal, and ensemble expansion define the key dimensions of AI-enabled molecular simulation, as discussed in the following sections.

4.2.1. *Configurational expansion*

Configurational expansion addresses the combinatorial growth of atomic arrangements in multicomponent and structurally heterogeneous catalysts [152]. In systems such as high-entropy alloys (HEAs), defect-rich interfaces, and nanocrystalline-amorphous (N/A) composites, the number of distinct surface sites increases exponentially with compositional and structural complexity [153]. Conventional DFT approaches typically evaluate a limited set of representative slab models and adsorption sites, which restricts mechanistic interpretation to a small subset of the accessible configuration space [154].

To overcome this limitation, Li *et al.* employed an atomistic line graph neural network (ALIGNN)-based MLP for MC to enable large-scale equilibrium sampling of a HEA surface [149]. Canonical Monte Carlo (cMC) simulations driven by the trained potential were used to determine thermodynamically equilibrated surface segregation profiles, shown in Fig. 8d. The results reveal preferential enrichment of specific elements at the outermost layer, establishing the physically relevant

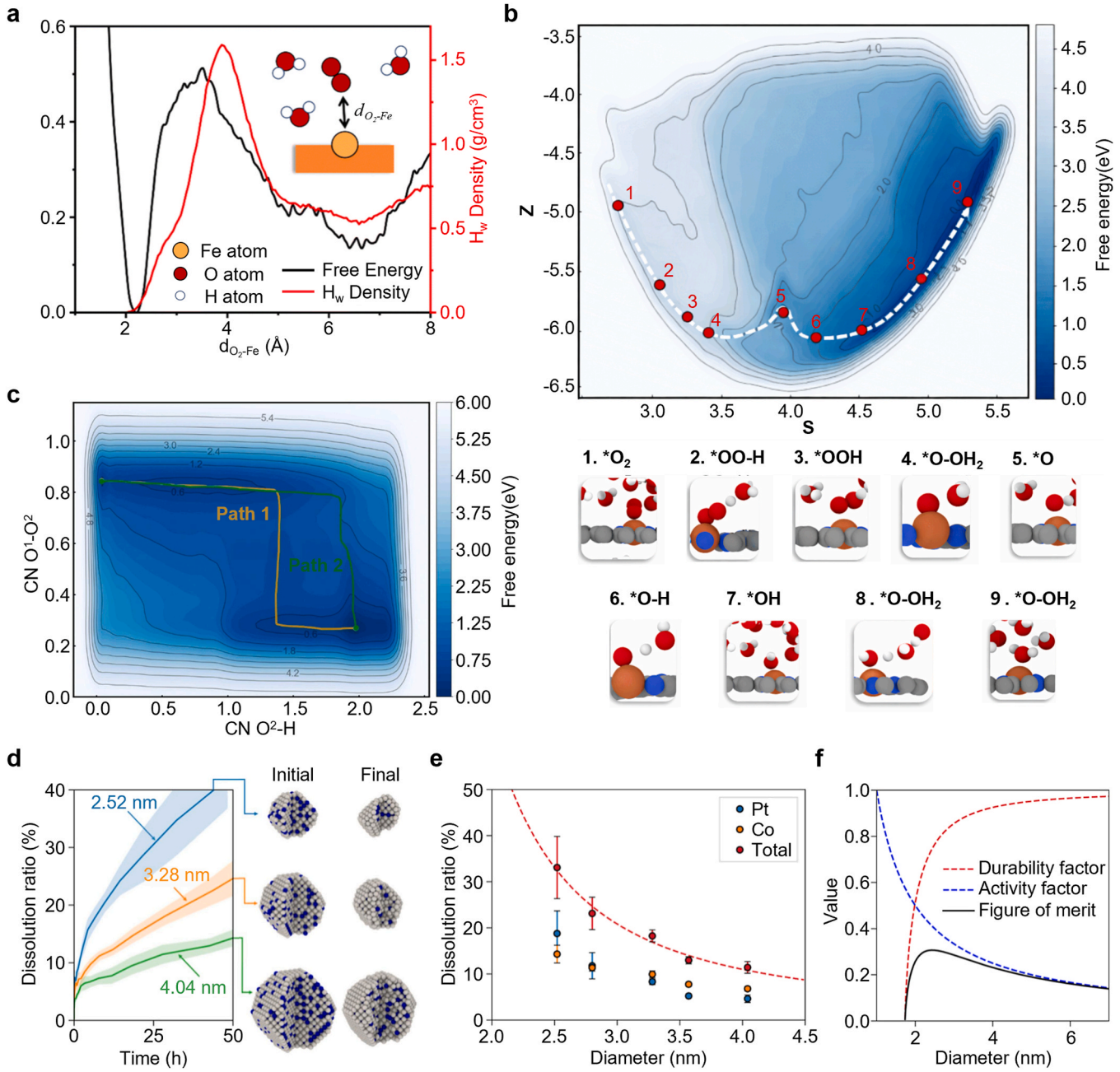

Fig. 9. a) Free-energy profile for O_2 adsorption on an Fe–N_4/C catalyst in fully explicit water, reconstructed using a MLFF combined with metadynamics. b) Global free-energy surface projected onto path collective variables, explicitly resolving the minimum-energy pathway of the ORR. c) Extended nanosecond-scale sampling of PCET pathways, distinguishing barrierless steps from the rate-determining O_2 adsorption process. Reproduced with permission from Ref. [155]. Copyright 2025 The Royal Society of Chemistry. d) Time evolution of the dissolution ratio for varying sizes of Pt_3Co nanoparticles, obtained via NNP-driven off-lattice kMC simulations. e) Diameter dependence of the dissolution ratio, demonstrating that smaller nanoparticles exhibit higher dissolution propensity. f) Combined activity–durability analysis establishing a FOM that captures the trade-off between catalytic activity and structural stability as a function of nanoparticle size. Reproduced with permission from Ref. [156]. Copyright 2023 American Chemical Society.

surface configuration under reaction-relevant conditions [149]. Using these equilibrated structures, they predicted site-resolved OH adsorption energies with a pretrained neural network model and mapped them onto a volcano-based electrokinetic framework for ORR [149]. The resulting activity map and adsorption energy histograms (Fig. 8e) exhibit a broad distribution of adsorption free energies, with a substantial fraction of sites positioned near the volcano apex. These results show that ORR enhancement correlates with a segregation-induced shift in the adsorption energy distribution, increasing the statistical population of near-optimal sites rather than generating a single dominant active motif.

A comparable configurational strategy was applied to structurally heterogeneous nanocrystalline–amorphous (N/A) interfaces by Huang *et al.* [150]. A high-dimensional neural network potential (HDNNP), developed based on deep potential generator (DP-GEN), enabled large-scale MD simulations of interfacial structures beyond DFT-accessible system sizes. After structural equilibration, adsorption free energies were evaluated across crystalline, interfacial, and amorphous regions within the computational hydrogen electrode framework [150]. The fraction of sites located within ±0.3 eV of the volcano-top descriptor is shown in Fig. 8b, where interfacial domains exhibit the highest active-site population. The corresponding distributions of ΔG_{O^*}

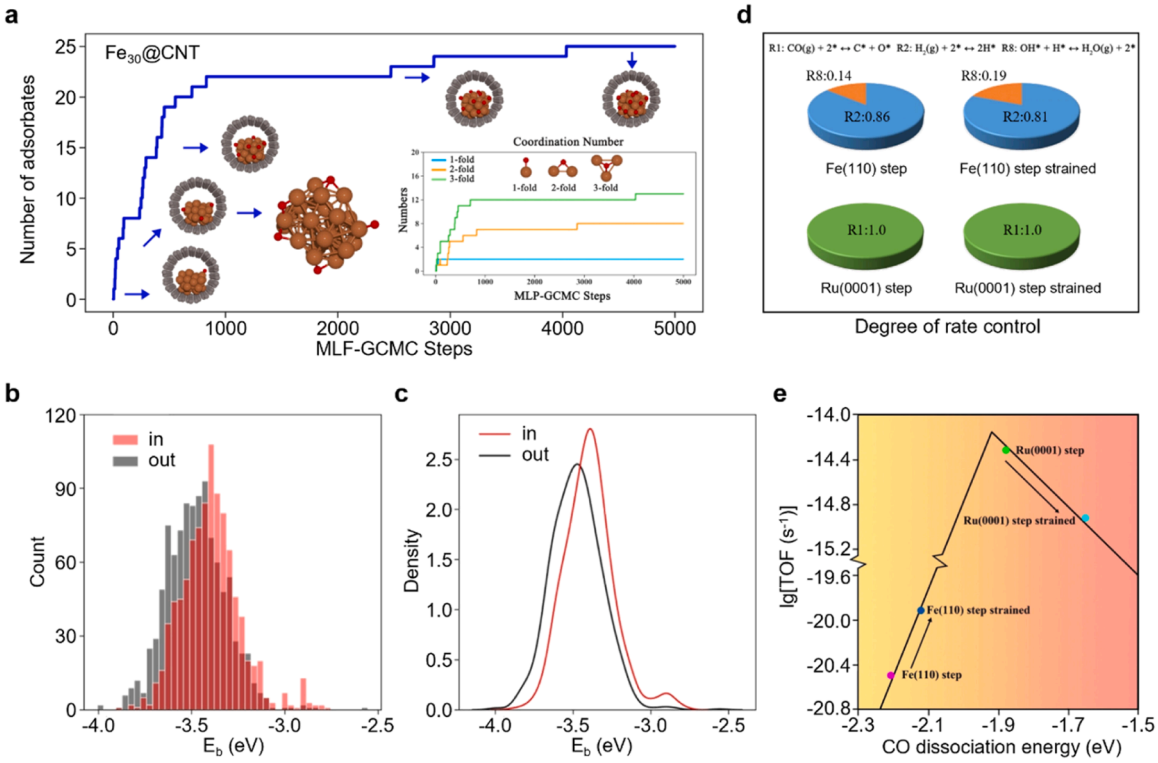

Fig. 10. a) Dynamic oxygen adsorption and structural evolution of an Fe_{30} cluster confined within a CNT during MLP-GCMC simulations. b) Histogram of the oxygen binding energy distributions for the confined and supported Fe clusters. c) KDE of the binding energies, revealing a systematic shift toward weaker binding under CNT confinement. d) DRC analysis for Fe and Ru step surfaces with and without compressive strain, simulating the structural effects of confinement. e) Volcano plot for the TOF of CO conversion versus CO dissociation energy, demonstrating how confinement-induced binding energy shifts lead to distinct kinetic responses depending on the catalyst. Reproduced with permission from Ref. [160]. Copyright 2025 John Wiley and Sons.

$-\Delta G_{VTO^*}$ (Fig. 8c) indicate both a shift of the mean toward the volcano apex and broader dispersion at the interface. Huang *et al.* thereby quantified how structural disorder increases the probability of generating near-optimal adsorption configurations for OER.

Across these studies, AI-enabled configurational sampling establishes a direct connection between equilibrium structure and statistical activity distributions. In HEA systems, Li *et al.* demonstrated that compositional segregation shifts adsorption energetics toward the volcano apex. In N/A interfaces, Huang *et al.* showed that structural heterogeneity broadens and re-centers adsorption energy distributions. Thus, configurational expansion reframes mechanistic analysis from isolated active-site identification to ensemble-level evaluation of catalytically favorable configurations across large atomic populations.

4.2.2. *Temporal expansion*

Temporal expansion addresses the fundamental limitation of time resolution in first-principles molecular simulations of electrocatalytic systems [153]. Electrochemical reactions at solid–liquid interfaces are governed by rare barrier-crossing events, solvent reorganization, and dynamic restructuring processes that occur over nanosecond or longer timescales [152,154]. Conventional AIMD simulations typically access only picosecond trajectories, which constrains transition-state sampling, limits free-energy convergence, and prevents statistically meaningful characterization of solvent fluctuations or degradation kinetics. Machine-learning force fields (MLFFs) overcome this bottleneck by learning the underlying potential energy surface from first-principles data, thereby enabling long-time MD with near-DFT accuracy [153].

The impact of temporal expansion is evident in kinetic investigations of the ORR at explicit solid–liquid interfaces [155]. Using an active-learning MLFF framework combined with well-tempered metadynamics, Yu *et al.* reconstructed the free-energy landscape of ORR on Fe–N_4/C in fully explicit water [155]. The free-energy profile for O_2 adsorption as a function of the O_2–Fe distance (Fig. 9a) reveals a barrier of 0.39 eV. The global free-energy surface projected onto path collective variables (S, Z), shown in Fig. 9b, explicitly resolves reactants, intermediates, transition states, and products along the minimum-energy pathway. Extended sampling further enabled resolution of competing proton-coupled electron transfer (PCET) pathways (Fig. 9c), distinguishing barrierless PCET steps from the rate-determining O_2 adsorption process. Nanosecond-scale trajectories provided statistically converged hydrogen-bond distributions and lifetimes at the interface, directly linking solvent microstructure to kinetic barriers [155]. Such solvent-resolved kinetic coupling cannot be reliably captured within short AIMD trajectories.

Temporal expansion further enables direct resolution of degradation kinetics that evolve beyond the time window accessible to conventional ab initio simulations [156]. In alloy nanoparticles, structural instability and dissolution arise from slow atomic detachment and surface rearrangement processes that require extended sampling to capture statistically meaningful trends [156]. Using machine-learned interatomic potentials, Jung *et al.* performed long-time MD simulations to quantify dissolution behavior of truncated octahedral Pt_3Co nanoparticles with varying diameters [156]. The time evolution of the dissolution ratio, defined as the fraction of dissolved atoms relative to the initial total atom count, is shown in Fig. 9d. These trajectories reveal progressive size-dependent degradation behavior over simulated long-time intervals. The diameter dependence of the dissolution ratio after 24 h equivalents (Fig. 9e) demonstrates a clear scaling relationship, with smaller nanoparticles exhibiting higher dissolution propensity.

By integrating these degradation metrics with geometric activity scaling (activity factor $\propto 1/d$), Jung *et al.* constructed a combined activity–durability analysis (Fig. 9f). The resulting figure of merit (FOM) quantitatively captures the trade-off between catalytic activity and structural stability as a function of nanoparticle size. This

Table 4
Dimensional expansion enabled by AI in atomistic electrocatalysis.

	Reaction / Catalysts	AI Model	Simulation Framework	Expanded Dimension	Key Mechanistic Insight	Ref.
Configurational expansion	ORR / HEA	ALIGNN + TinNet	MC + adsorption ML	Configuration space	Site distribution shifts adsorption energy distribution toward volcano apex	[149]
	OER / Interface	HDNNP	Large-scale structure sampling	Structural heterogeneity	Interface increases fraction of near-optimal adsorption sites	[150]
Temporal expansion	ORR / Fe-N4/C	MLFF (DeepMD)	MLFF-MD + MetaD	Time (rare-event kinetics)	Explicit solvent-dependent free energy barrier and RDS identification	[155]
	ORR / Pt_3Co	MLP (NNP)	Off-lattice kMC	Time (degradation evolution)	Dissolution kinetics and morphology-durability tradeoff	[156]
Ensemble expansion	CNT confinement	MLP (REANN)	MLP-GCMC + microkinetics	Thermodynamic ensemble	Binding energy distribution shift and activity reversal via strain-induced d-band shift	[160]

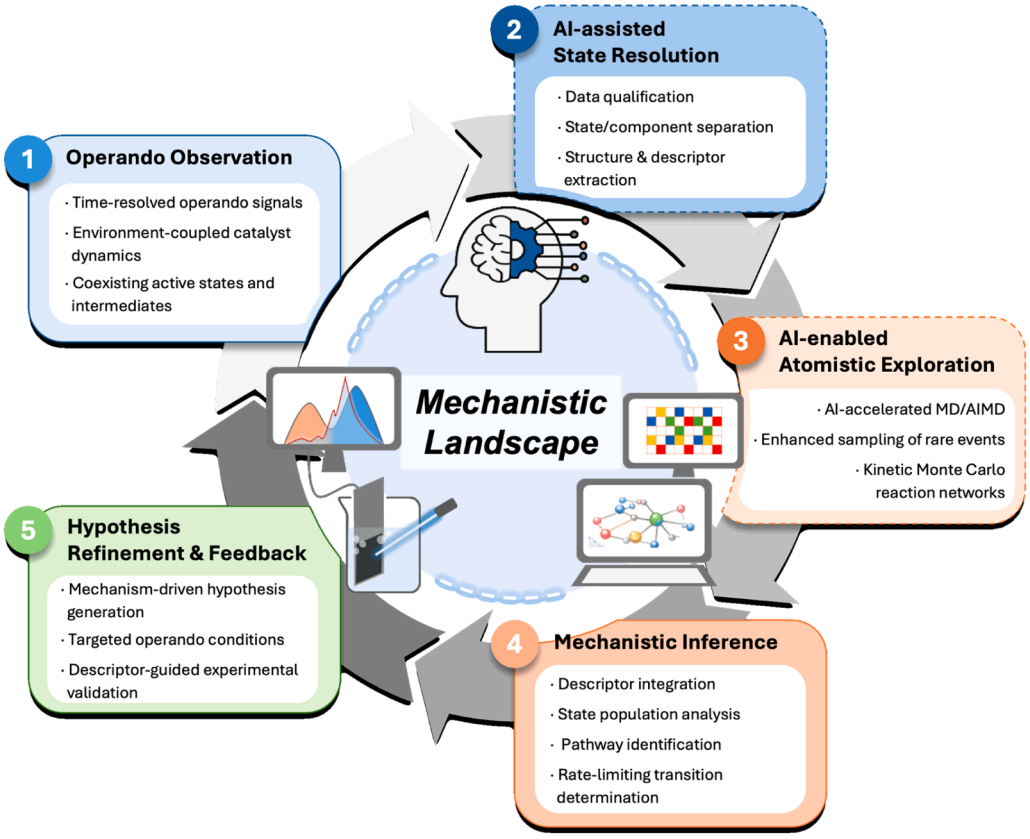

Fig. 11. Unified AI-driven closed-loop framework for mechanism discovery in electrocatalysis.

stability–activity relationship emerges from explicitly sampling degradation pathways over extended timescales, illustrating how temporal expansion enables mechanistic evaluation of long-term catalyst performance rather than short-time energetic snapshots [156].

Through these studies, temporal expansion facilitates statistically converged free-energy surfaces, explicit identification of rate-determining steps, and direct observation of slow degradation pathways. In interfacial ORR, extended sampling resolves solvent-controlled kinetic barriers. In alloy nanoparticles, long-time evolution reveals size-dependent dissolution mechanisms and structural instability. Thus, temporal expansion shifts atomistic modeling from short-time energetic snapshots to time-resolved kinetic and durability analysis under realistic electrochemical conditions.

4.2.3. *Ensemble expansion*

Ensemble expansion addresses a fundamental thermodynamic limitation in conventional first-principles catalyst modeling. Standard DFT approaches typically evaluate adsorption energetics on a single optimized structure at fixed coverage, implicitly assuming that one representative configuration governs catalytic behavior [157]. Under realistic reaction conditions, however, catalysts exist as thermodynamic ensembles defined by finite temperature, variable chemical potentials, fluctuating coverages, and dynamically evolving coordination environments [158]. Reactivity therefore reflects the statistical distribution of accessible states rather than the properties of a single minimum-energy geometry. AI-enabled simulation frameworks make it possible to explicitly construct and analyze such ensembles [157,159].

This shift is exemplified by the MLP-accelerated GCMC simulations reported by Yang *et al.*, where confined Fe nanoparticles inside carbon nanotubes (CNTs) were studied under operando atmospheres [160]. In this approach, machine-learned interatomic potentials trained on AIMD data enabled large-scale sampling, while GCMC incorporated temperature and chemical potential effects. As illustrated in Fig. 10a, oxygen adsorption on Fe_{30} clusters evolves dynamically with increasing coverage, and the O–Fe coordination number continuously reorganizes during sampling. Adsorption sites are not static; newly introduced

adsorbates induce redistribution of previously stabilized species, generating a population of metastable configurations. This behavior demonstrates that the catalytically relevant structure is inherently ensemble-defined.

The ensemble character becomes explicit when adsorption energetics are evaluated statistically [160]. Rather than comparing single adsorption energies, Yang *et al.* analyzed hundreds of sampled configurations to construct binding-energy histograms and kernel density estimates (Fig. 10b, c). The distributions reveal a systematic shift of approximately 0.2 eV toward weaker binding for Fe clusters confined inside CNTs relative to supported counterparts. Importantly, this confinement effect manifests as a displacement of the entire probability distribution rather than as an isolated structural anomaly [160]. The trend persists across temperatures, nanoparticle sizes, and reacting species, indicating that confinement modifies the ensemble-averaged electronic environment.

To elucidate the structural origin of this distribution-level modulation, Yang *et al.* applied Random Forest regression to more than 20,000 sampled configurations [160]. Feature-importance analysis identified average Fe–Fe bond length as the dominant descriptor governing adsorption energy variations, followed by coordination statistics and Fe–C interfacial bonding. Confinement induces slight but systematic bond-length shortening, corresponding to compressive strain within encapsulated clusters [160]. Electronic structure analysis further shows a downshift of the d-band center for confined systems, rationalizing the weakened adsorption energies in terms of modified antibonding occupation. Through this data-driven analysis, ensemble sampling is linked quantitatively to structural and electronic descriptors [160].

The ensemble perspective also enables direct integration with kinetic modeling. Using strain-modified slab models to represent confinement-induced bond shortening, microkinetic simulations and degree-of-rate-control (DRC) analysis were performed (Fig. 10d) [160]. The weakened adsorption energies derived from ensemble statistics produce catalyst-dependent kinetic responses: for Fe surfaces, reduced binding alleviates surface poisoning and enhances activity, whereas for Ru surfaces the same energetic shift increases the barrier for reactant dissociation and suppresses activity. The seemingly contradictory experimental observations of enhanced and suppressed confined catalysis thus emerge naturally from volcano-type kinetic sensitivity. Ensemble expansion therefore connects thermodynamic sampling to reaction-rate control within a unified framework.

By combining machine-learned potentials, grand canonical sampling, statistical analysis, and microkinetic modeling, ensemble expansion transforms atomistic simulation into a thermodynamically consistent description of operando catalysis. Reactivity is no longer interpreted through a single adsorption energy, but rather through shifts in probability distributions governed by structural strain and electronic modulation. In this framework, AI does not merely accelerate computation; it enables explicit resolution of the statistical state space that defines catalytic function under realistic chemical potentials (Table 4).

5. Conclusion and perspective

Electrocatalysis proceeds under inherently dynamic, non-equilibrium conditions in which catalytic performance emerges from continuously evolving active states, transient intermediates, and environment-coupled interfacial interactions. As highlighted throughout this review, mechanistic understanding in such systems cannot be reduced to static structural descriptors or isolated minimum-energy pathways. Instead, it requires analytical frameworks capable of resolving heterogeneous, time-dependent, and ensemble-defined catalytic states under realistic operating conditions.

AI contributes to this challenge not by replacing physical insight, but by enhancing mechanistic resolution across both experimental and theoretical domains. In operando electrocatalysis, AI-driven data qualification, state separation, and structural inference enable transformation of high-dimensional measurements into statistically and structurally interpretable state representations. In atomistic simulations, AI-enabled configurational, temporal, and ensemble expansion extends the accessible state space of molecular modeling, allowing statistically grounded exploration of catalytic landscapes beyond the intrinsic of conventional approaches. Together, these parallel developments redefine mechanistic inquiry from single-state analysis toward dynamic state-space exploration.

The unified framework illustrated in Fig. 11 encapsulates this transition toward an AI-integrated, closed-loop paradigm for mechanism discovery. In this workflow, operando observations generate high-dimensional representations of evolving catalytic systems; AI-driven analysis resolves these observations into interpretable states; AI-enabled simulations explore the broader configurational and kinetic landscape; and mechanistic inference integrates these insights to generate targeted hypotheses. Iterative feedback between experiment and simulation progressively refines state representations and reaction pathways, forming a self-consistent cycle of hypothesis generation, validation, and refinement. By embedding AI within experimentally anchored and theory-guided workflows, electrocatalysis research can move beyond descriptive characterization toward predictive, mechanism-driven understanding. Such integration holds the potential to accelerate rational catalyst design by systematically resolving the dynamic complexity that defines catalytic function under operating conditions. Ultimately, this AI-integrated paradigm provides a roadmap for designing next-generation catalysts with unprecedented efficiency and selectivity, bridging the gap between fundamental understanding and practical application. In addition, it enables the prediction of mechanistic phenomena, guiding hypothesis generation and offering a pathway toward rational, predictive catalyst design. This framework could accelerate discovery across energy conversion technologies.

CRediT authorship contribution statement

Junyoung Mun: Validation, Supervision. **Jung Ho Kim:** Validation, Supervision, Project administration. **Hun-Gi Jung:** Validation, Supervision. **Jongsoon Kim:** Validation, Supervision. **Jiwon Kim:** Writing – review & editing, Writing – original draft, Visualization, Conceptualization. **Sangkyu Woo:** Writing – original draft, Visualization.

Declaration of Competing Interest

The authors declare that they have no known competing financial interests or personal relationships that could have appeared to influence the work reported in this paper.

Acknowledgements

This work was supported by the Ministry of Trade, Industry & Energy/Korea Evaluation Institute of Industrial Technology (MOTIE/KEIT) (RS-2025-25458436), the National R&D Program through the National Research Foundation of Korea (NRF) funded by the Ministry of Science and ICT (RS-2024-00408156) of Republic of Korea.

Data availability

No data was used for the research described in the article.

References

[1] X. Kong, J. Zhu, Z. Xu, Z. Geng, Fundamentals and challenges of ligand modification in heterogeneous electrocatalysis, Angew. Chem. Int Ed. Engl. 64 (2025) e202417562.
[2] C. Xie, W. Chen, Y. Wang, Y. Yang, S. Wang, Dynamic evolution processes in electrocatalysis: structure evolution, characterization and regulation, Chem. Soc. Rev. 53 (2024) 10852–10877.
[3] J. Kim, W.K. Pang, J. Mun, T. Song, J. Chen, J.H. Kim, D.H. Yoon, Prospect of ruthenium for hydrogen evolution reaction in alkaline media through in situ monitoring, Adv. Energy Mater. 15 (2025) 2502858.

[4] D.S. Aldianto Pratama, C.W. Lee, Electrocatalytic seawater splitting for sustainable hydrogen production: recent advances and material perspectives, J. Energy Chem. 117 (2026) 146–173.
[5] A. Li, H. Ooka, S. Kong, K. Adachi, Y. Zhang, K. Fushimi, S. Hamamoto, M. Oura, S.H. Kim, D. Hashizume, R. Nakamura, Oxygen evolution electrocatalysis resilient to voltage fluctuations, Nat. Sustain. 8 (2025) 1533–1540.
[6] N. Sakamoto, K. Sekizawa, S. Sato, J. Jung, T. Wakabayashi, K. Kamada, T. Nonaka, T. Uyama, T. Morikawa, S. Saito, Mechanism of CO_2 Electrolysis with Heterogenized Molecular Iridium Catalysts Deciphered Using Operando Spectroscopy, J. Am. Chem. Soc. 147 (2025) 47859–47866.
[7] Y. Zhang, T. Binninger, J. Huang, M. Eikerling, Effective Ion Concentration as a Descriptor for the Local Reaction Environment at Nanoparticle-Based Electrocatalysts, ACS Catal. 16 (2026) 3175–3187.
[8] X. Ding, X. Fu, Dynamic reconstruction defines true active states in the hydrogen evolution reaction, Energy & Environ. Sci. 19 (2026) 1497–1507.
[9] H. Liu, X. Liu, A. Sun, C. Xuan, Y. Ma, Z. Zhang, H. Li, Z. Wu, T. Ma, J. Wang, Enhancing Oxygen Evolution Electrocatalysis in Heazlewoodite: Unveiling the Critical Role of Entropy Levels and Surface Reconstruction, Adv. Mater. 37 (2025) e2501186.
[10] C.H. Scharf, A. Chandraraj, K. Dyk, F. Stebner, S. Lepin, J. Tian, L. El Bergmi Byaz, J. Stettner, C. Leppin, A. Kotova, S. Reinke, J. Linnemann, F. Maroun, O. M. Magnussen, Role of Defects in Reversible Surface Restructuring and Activity of Co_3O_4 Oxygen Evolution Electrocatalysts, ACS Catal. 16 (2026) 4877–4891.
[11] Q. Tang, S. Zhang, B. Zhu, Y. Gao, Situ Reconstruction of a Cu(100) Surface for Promoted C–C Coupling in CO_2 Electroreduction from First-Principles Multiscale Modeling, ACS Catal. 16 (2026) 1325–1337.
[12] Q. Wang, Y.B. Liao, B. Mei, J. Zhang, D. Kido, W. Cheng, G. Chen, T. Zhang, Y. Cao, S.L. Li, Y. Yan, Y.Q. Lan, Operando XAFS Reveals Dynamic Structural Evolution of Pt Single-Atom Catalysts for Efficient Chlorine Electrosynthesis, Angew. Chem. Int Ed. Engl. 64 (2025) e202513656.
[13] D.J. Zheng, K. McCormack, J. Peng, R. Garcia-Diez, E.Y. Kataev, F. Schwarz, S. Nehzati, J. Thyr, W. Quevedo-Garzon, B. Howchen, M. Bar, Y. Roman-Leshkov, Y. Shao-Horn, M. Gorlin, Lattice Oxygen Exchange Pathways in Nickel-Iron Metal-Organic Framework-Based Oxygen Evolution Electrocatalysts, ACS Appl. Mater. Interfaces 18 (2026) 1062–1076.
[14] H.W. Choi, H. Lee, J. Lu, S. Bin Kwon, D.I. Jeong, B.J. Park, J. Kim, B.K. Kang, G. Jang, D.H. Yoon, Trifunctional robust electrocatalysts based on 3D Fe/N-doped carbon nanocubes encapsulating Co_4N nanoparticles for efficient battery-powered water electrolyzers, Carbon Energy 6 (2024) e505.
[15] J. Bai, Z. Dong, X. Jiang, Q. Zhou, J. Zhao, J. Mei, Z. Tan, T. Liao, Z. Sun, Advancing Nitrate-to-Ammonia Electrocatalysis: Strategies in Catalyst Design, Electrolyte Engineering, and Performance Evaluation, Adv. Sci. 12 (2025) e08614.
[16] P. Sebastián-Pascual, A. Herzog, Y. Zhang, Y. Shao-Horn, M. Escudero-Escribano, Electrolyte effects in proton–electron transfer reactions and implications for renewable fuels and chemicals synthesis, Nat. Catal. 8 (2025) 986–999.
[17] P.-P. Wang, H.-B. Chi, W.-F. Yang, X.-F. Zhao, G.-F. Long, Z.-P. Yu, Interfacial electrolyte effects on electrocatalytic oxygen evolution reaction, Rare Met. 44 (2025) 8329–8355.
[18] B.W.J. Chen, M. Mavrikakis, Modeling the impact of structure and coverage on the reactivity of realistic heterogeneous catalysts, Nat. Chem. Eng. 2 (2025) 181–197.
[19] X. Chen, Y.L. Sun, X.M. Lin, J.C. Dong, J.F. Li, situ Studies of Electrochemical Energy Conversion and Storage Technologies: From Materials, Intermediates, and Products to Surroundings, Nanomicro Lett. 18 (2026) 160.
[20] K. Dong, S. Han, Y. Li, Z. Wang, C. Xue, X. Sun, Y. Yao, H. Li, X. Wang, D. Ma, L. M. Liu, B. Zhang, Testing, quantification, in situ characterization and calculation simulation for electrocatalytic nitrate reduction, Nat. Protoc. (2025).
[21] Z. Huang, D. Eder, Harnessing the structural evolution of metal-organic frameworks under electrocatalytic conditions, Commun. Chem. 8 (2025) 359.
[22] R. Sun, X. Liu, J. Huang, Y. Wang, H. Huang, Y. Lei, J. Ge, Situ and Operando Analytical Techniques of Single-Atom Catalysts for Electrocatalytic CO_2 Reduction, Small Methods 9 (2025) e2500516.
[23] D. Chen, Y. Wei, Z. Sun, X. Zhao, X. Tang, X. Zhu, G. Li, L. Yao, S. Chen, R. Lin, J. Wang, Q. Li, X. Fan, T. Qiu, Q. Hao, Unveiling the Cation Effects on Electrocatalytic CO_2 Reduction via Operando Surface-enhanced Raman Spectroscopy, Small 21 (2025) e2409569.
[24] M. Shi, F. Sultana, X. Qin, P. Zhang, K. Qian, T. Wei, Y. Duan, T. Li, J. Bai, R. Li, situ evolution of MOF-derived C@NiCoP/NF promotes urea-assisted electrocatalytic hydrogen production, Appl. Catal. B Environ. Energy 371 (2025) 125210.
[25] W. Yu, S. Yue, M. Yang, M. Hashimoto, P. Liu, L. Zhu, W. Xie, T. Jones, M. Willinger, X. Huang, Operando TEM study of a working copper catalyst during ethylene oxidation, Nat. Commun. 16 (2025) 2029.
[26] D. Cheng, K.C. Nguyen, V. Sumaria, Z. Wei, Z. Zhang, W. Gee, Y. Li, C.G. Morales-Guio, M. Heyde, B. Roldan Cuenya, A.N. Alexandrova, P. Sautet, Structure Sensitivity and Catalyst Restructuring for CO_2 Electro-reduction on Copper, Nat. Commun. 16 (2025) 4064.
[27] Y. Xu, H. Li, J. Yang, Y. Liu, W. Deng, A. Lee, F. Jiao, F. Che, Active learning-guided catalyst design for selective acetate production in CO electroreduction, Nat. Commun. 16 (2025) 11503.
[28] X. Jin, T. Lee, J. Park, J. Kim, S. Park, S.Y. Yun, Y.E. Sung, D.W. Kim, M.G. Kim, A. Soon, S.J. Hwang, pH-dependent mechanism of oxygen evolution in highly disordered RuO_2 nanosheets, Nat. Commun. 17 (2025) 672.
[29] A. Prajapati, C. Hahn, I.M. Weidinger, Y. Shi, Y. Lee, A.N. Alexandrova, D. Thompson, S.R. Bare, S. Chen, S. Yan, N. Kornienko, Best practices for in-situ and operando techniques within electrocatalytic systems, Nat. Commun. 16 (2025) 2593.
[30] Z. Levell, J. Le, S. Yu, R. Wang, S. Ethirajan, R. Rana, A. Kulkarni, J. Resasco, D. Lu, J. Cheng, Y. Liu, Emerging Atomistic Modeling Methods for Heterogeneous Electrocatalysis, Chem. Rev. 124 (2024) 8620–8656.
[31] A.O. Elnabawy, M. Mavrikakis, Nanocluster Active Sites Formed on Heterogeneous Thermal Catalysts and Electrocatalysts by Operando Reactive Environments, ACS Catal. 15 (2025) 9919–9927.
[32] H. Bae, H. Ji, K. Konstantinov, R. Sluyter, K. Ariga, Y.H. Kim, J.H. Kim, Artificial Intelligence-Driven Nanoarchitectonics for Smart Targeted Drug Delivery, Adv. Mater. 37 (2025) e10239.
[33] T.H. Lee, S. Lee, L. Yuan, J.A. Dionne, J. Park, Integrative Approaches to Reveal Catalyst Dynamics: Bridging Operando Techniques, Theory, and Artificial Intelligence, ACS nano 19 (2025) 36827–36844.
[34] Y. Zeng, J. Wang, F. Li, T. Liu, A. Xu, AI-Accelerated Discovery of Electrocatalyst Materials, ACS Mater. Au 6 (2026) 72–89.
[35] L. Xu, J. Zhou, A.S. Bandarenka, Z. Chen, Data-Driven Electrocatalyst Discovery: Recent Trends in Machine Learning Approaches and Descriptor-Based Design Principles, Acc. Mater. Res. 7 (2026) 294–308.
[36] X. Lin, W. Qu, Z. Wang, J. Liu, C. Qian, L. Tian, L. Wang, Y. Zhang, H. Zhou, Y. Zhao, Y. Wu, Decoding heterogeneous electrocatalysts for acidic oxygen evolution: mechanisms, rational design and AI acceleration, Natl. Sci. Rev. 12 (2025) nwaf474.
[37] Y.B. Zhuang, C. Liu, J.X. Zhu, J.Y. Hu, J.B. Le, J.Q. Li, X.J. Wen, X.T. Fan, M. Jia, X.Y. Li, A. Chen, L. Li, Z.L. Lin, W.H. Xu, J. Cheng, An artificial intelligence accelerated ab initio molecular dynamics dataset for electrochemical interfaces, Sci. Data 12 (2025) 997.
[38] Y. Yang, J. Feijóo, M. Figueras-Valls, C. Chen, C. Shi, M.V. Fonseca Guzman, Y. Murhabazi Maombi, S. Liu, P. Jain, V. Briega-Martos, Z. Peng, Y. Shan, G. Lee, M. Rebarchik, L. Xu, C.J. Pollock, J. Jin, N.E. Soland, C. Wang, M.B. Salmeron, Z. Chen, Y. Han, M. Mavrikakis, P. Yang, Operando probing dynamic migration of copper carbonyl during electrocatalytic CO_2 reduction, Nat. Catal. 8 (2025) 579–594.
[39] T.T. Yang, W.A. Saidi, Machine Learning-Accelerated First-Principles Molecular Dynamics Reveals C–C Coupling Mechanisms toward Ethylene on Cu(100), ACS Catal. 15 (2025) 15093–15101.
[40] Y. Tang, C. Wu, Q. Zhang, H. Zhong, A. Zou, J. Li, Y. Ma, H. An, Z. Yu, S. Xi, J. Xue, X. Wang, J. Wu, Accelerated Surface Reconstruction through Regulating the Solid-Liquid Interface by Oxyanions in Perovskite Electrocatalysts for Enhanced Oxygen Evolution, Angew. Chem. Int Ed. Engl. 62 (2023) e202309107.
[41] A. Prajapati, C. Hahn, I.M. Weidinger, Y. Shi, Y. Lee, A.N. Alexandrova, D. Thompson, S.R. Bare, S. Chen, S. Yan, Best practices for in-situ and operando techniques within electrocatalytic systems, Nat. Commun. 16 (2025) 2593.
[42] B. Roldán Cuenya, M.A. Bañares, Introduction: Operando and in situ studies in catalysis and electrocatalysis, 124, ACS Publications, 2024, pp. 8011–8013.
[43] S. Zuo, Z.P. Wu, H. Zhang, X.W. Lou, Operando monitoring and deciphering the structural evolution in oxygen evolution electrocatalysis, Adv. Energy Mater. 12 (2022) 2103383.
[44] F. Domínguez-Flores, M.M. Melander, Electrocatalytic rate constants from DFT simulations and theoretical models: Learning from each other, Curr. Opin. Electrochem. 36 (2022) 101110.
[45] T.D. Dolezal, A.J. Samin, Adsorption of Oxygen to High Entropy Alloy Surfaces for up to ML Coverage Using Density Functional Theory and Monte Carlo Calculations, Langmuir 38 (2022) 3158–3169.
[46] Y. Zhu, J. Wang, H. Chu, Y.-C. Chu, H.M. Chen, In situ/operando studies for designing next-generation electrocatalysts, ACS Energy Lett. 5 (2020) 1281–1291.
[47] J. Li, J. Gong, Operando characterization techniques for electrocatalysis, Energy & Environ. Sci. 13 (2020) 3748–3779.
[48] S. Choi, J. Kwon, J. Kim, J. Sun, C. Park, G.N. Jameson, J.H. Kim, U. Paik, T. Song, Independent-active-site engineering in N: NiFeP@ FeNC electrocatalyst for mitigating HER site oxidation in alkaline electrolysis, Adv. Compos. Hybrid. Mater. 8 (2025) 438.
[49] H. Jiang, Q. He, Y. Zhang, L. Song, Structural self-reconstruction of catalysts in electrocatalysis, Acc. Chem. Res. 51 (2018) 2968–2977.
[50] H.N. Nong, T. Reier, H.-S. Oh, M. Gliech, P. Paciok, T.H.T. Vu, D. Teschner, M. Heggen, V. Petkov, R. Schlögl, A unique oxygen ligand environment facilitates water oxidation in hole-doped $IrNiO_x$ core–shell electrocatalysts, Nat. Catal. 1 (2018) 841–851.
[51] W. Zhu, W. Chen, H. Yu, Y. Zeng, F. Ming, H. Liang, Z. Wang, NiCo/NiCo–OH and NiFe/NiFe–OH core shell nanostructures for water splitting electrocatalysis at large currents, Appl. Catal. B Environ. 278 (2020) 119326.
[52] A. Jahandoost, R. Dashti, M. Houshmand, S.A. Hosseini, Utilizing machine learning and molecular dynamics for enhanced drug delivery in nanoparticle systems, Sci. Rep. 14 (2024) 26677.
[53] H. Cao, Q. Wang, Z. Zhang, H.M. Yan, H. Zhao, H.B. Yang, B. Liu, J. Li, Y. G. Wang, Engineering Single-Atom Electrocatalysts for Enhancing Kinetics of Acidic Volmer Reaction, J. Am. Chem. Soc. 145 (2023) 13038–13047.
[54] S. Choi, H. Lee, J. Kwon, J. Sun, G. Ali, L. Olivi, N. Imam, J. Choi, J.H. Kim, H. Han, Elucidating mechanism of Se-induced lattice oxygen activation and structural stability in perovskite oxide for oxygen evolution catalysis, J. Power Sources 657 (2025) 238152.
[55] A. Kumar, M. Gil-Sepulcre, J.P. Fandre, O. Rudiger, M.G. Kim, S. DeBeer, H. Tuysuz, Regulating Local Coordination Sphere of Ir Single Atoms at the Atomic Interface for Efficient Oxygen Evolution Reaction, J. Am. Chem. Soc. 146 (2024) 32953–32964.

[56] S. Chen, L. Ma, Z. Huang, G. Liang, C. Zhi, situ/operando analysis of surface reconstruction of transition metal-based oxygen evolution electrocatalysts, Cell Rep. Phys. Sci. 3 (2022) 100729.

[57] Y. Hu, Y. Zheng, J. Jin, Y. Wang, Y. Peng, J. Yin, W. Shen, Y. Hou, L. Zhu, L. An, M. Lu, P. Xi, C.H. Yan, Understanding the sulphur-oxygen exchange process of metal sulphides prior to oxygen evolution reaction, Nat. Commun. 14 (2023) 1949.

[58] Q. Zhang, Z. Song, X. Sun, Y. Liu, J. Wan, S.B. Betzler, Q. Zheng, J. Shangguan, K. C. Bustillo, P. Ercius, P. Narang, Y. Huang, H. Zheng, Atomic dynamics of electrified solid-liquid interfaces in liquid-cell TEM, Nature 630 (2024) 643–647.

[59] S. Kim, J. Kwag, M. Lee, S. Kang, D. Kim, J.G. Oh, Y.J. Heo, J. Ryu, J. Park, Unraveling Serial Degradation Pathways of Supported Catalysts through Reliable Electrochemical Liquid-Cell TEM Analysis, J. Am. Chem. Soc. 147 (2025) 181–191.

[60] Y. Yang, S. Louisia, S. Yu, J. Jin, I. Roh, C. Chen, M.V. Fonseca Guzman, J. Feijoo, P.C. Chen, H. Wang, C.J. Pollock, X. Huang, Y.T. Shao, C. Wang, D.A. Muller, H. D. Abruna, P. Yang, Operando studies reveal active Cu nanograins for CO_2 electroreduction, Nature 614 (2023) 262–269.

[61] Y. Qin, W. Zhao, C. Xia, L.J. Yu, F. Song, J. Zhang, T. Wu, R. Cao, S. Ding, B. Y. Xia, Y. Su, CO Intermediate-Assisted Dynamic Cu Sintering During Electrocatalytic CO_2 Reduction on Cu-N-C Catalysts, Angew. Chem. Int Ed. Engl. 63 (2024) e202404763.

[62] S. Li, S. Zhao, S.F. Hung, L. Deng, L. Wang, F. Shi, A. Dong, Y. Zhang, T.Y. Chen, F. Hu, L. Li, S. Ramakrishna, Y. Wu, S. Peng, Oxophilic Sites Mediated Dynamic Oxygen Replenishment to Stabilize Lattice Oxygen Catalysis in Acidic Water Oxidation, J. Am. Chem. Soc. 147 (2025) 33770–33779.

[63] Y. Li, J.L. Hart, R. Gawas, Z. Xia, P.P. Lopes, J. Zhang, S. Li, Y. Wang, M. Taheri, I. McCue, J. Snyder, Unveiling the Origin of Morphological Instability in Topologically Complex Electrocatalytic Nanostructures, J. Am. Chem. Soc. 147 (2025) 33482–33494.

[64] J. Kim, H.W. Choi, H. Choi, M.H. Han, S.B. Kwon, H.-S. Oh, H.Y. Kim, D.H. Yoon, Kinetic-oriented design of pyrrolic-N induced Ni and C dual sites for exceptional H_2O dissociation and alkaline HER, Appl. Catal. B Environ. Energy 357 (2024) 124324.

[65] M.A. Gebbie, B. Liu, W. Guo, S.R. Anderson, S.G. Johnstone, Linking electric double layer formation to electrocatalytic activity, Acs Catal. 13 (2023) 16222–16239.

[66] P. Li, Y. Jiao, J. Huang, S. Chen, Electric double layer effects in electrocatalysis: Insights from ab initio simulation and hierarchical continuum modeling, JACS Au 3 (2023) 2640–2659.

[67] R. Sundararaman, D. Vigil-Fowler, K. Schwarz, Improving the Accuracy of Atomistic Simulations of the Electrochemical Interface, Chem. Rev. 122 (2022) 10651–10674.

[68] T. Wu, C. Zhao, W. Chen, X. Sun, Y. Zhang, Atomic-Level Insights into the Cation-Mediated Electrocatalytic C-N Coupling Mechanism over Cu Model Catalyst, J. Phys. Chem. Lett. 17 (2026) 2418–2425.

[69] P.C. Chen, C. Chen, Y. Yang, A.L. Maulana, J. Jin, J. Feijoo, P. Yang, Chemical and Structural Evolution of AgCu Catalysts in Electrochemical CO_2 Reduction, J. Am. Chem. Soc. 145 (2023) 10116–10125.

[70] J. Halldin Stenlid, M. Gorlin, O. Diaz-Morales, B. Davies, V. Grigorev, D. Degerman, A. Kalinko, M. Borner, M. Shipilin, M. Bauer, A. Gallo, F. Abild-Pedersen, M. Bajdich, A. Nilsson, S. Koroidov, Operando Characterization of Fe in Doped $Ni_xFe_{(1-x)}O_yH_z$ Catalysts for Electrochemical Oxygen Evolution, J. Am. Chem. Soc. 147 (2025) 4120–4134.

[71] Y. Zhao, N. Dongfang, C. Huang, R. Erni, J. Li, H. Zhao, L. Pan, M. Iannuzzi, G. R. Patzke, Operando monitoring of the functional role of tetrahedral cobalt centers for the oxygen evolution reaction, Nat. Commun. 16 (2025) 580.

[72] M. Yan, R. Yang, C. Liu, Y. Gao, B. Zhang, situ probing the anion-widened anodic electric double layer for enhanced faradaic efficiency of chlorine-involved reactions, J. Am. Chem. Soc. 147 (2025) 6698–6706.

[73] P. Li, Y. Jiang, Y. Hu, Y. Men, Y. Liu, W. Cai, S. Chen, Hydrogen bond network connectivity in the electric double layer dominates the kinetic pH effect in hydrogen electrocatalysis on Pt, Nat. Catal. 5 (2022) 900–911.

[74] C. Rong, X. Huang, H. Arandiyan, Z. Shao, Y. Wang, Y. Chen, Advances in oxygen evolution reaction electrocatalysts via direct oxygen–oxygen radical coupling pathway, Adv. Mater. 37 (2025) 2416362.

[75] A. Herzog, M.Lopez Luna, H.S. Jeon, C. Rettenmaier, P. Grosse, A. Bergmann, B. Roldan Cuenya, Operando Raman spectroscopy uncovers hydroxide and CO species enhance ethanol selectivity during pulsed CO_2 electroreduction, Nat. Commun. 15 (2024) 3986.

[76] Y. Chen, C. Zhen, Y. Chen, H. Zhao, Y. Wang, Z. Yue, Q. Wang, J. Li, M.D. Gu, Q. Cheng, H. Yang, Oxygen Functional Groups Regulate Cobalt-Porphyrin Molecular Electrocatalyst for Acidic H_2O_2 Electrosynthesis at Industrial-Level Current, Angew. Chem. Int Ed. Engl. 63 (2024) e202407163.

[77] S. Yang, M. Jiang, W. Zhang, Y. Hu, J. Liang, Y. Wang, Z. Tie, Z. Jin, Situ Structure Refactoring of Bismuth Nanoflowers for Highly Selective Electrochemical Reduction of CO_2 to Formate, Adv. Funct. Mater. 33 (2023) 2301984.

[78] L. Xia, B.F. Gomes, W. Jiang, D. Escalera-Lopez, Y. Wang, Y. Hu, A.Y. Faid, K. Wang, T. Chen, K. Zhao, X. Zhang, Y. Zhou, R. Ram, B. Polesso, A. Guha, J. Su, C.M.S. Lobo, M. Haumann, R. Spatschek, S. Sunde, L. Gan, M. Huang, X. Zhou, C. Roth, W. Lehnert, S. Cherevko, L. Gan, F.P. Garcia de Arquer, M. Shviro, Operando-informed precatalyst programming towards reliable high-current-density electrolysis, Nat. Mater. 24 (2025) 753–761.

[79] Q. Hao, C. Zhen, Q. Tang, J. Wang, P. Ma, J. Wu, T. Wang, D. Liu, L. Xie, X. Liu, M.D. Gu, M.R. Hoffmann, G. Yu, K. Liu, J. Lu, Universal Formation of Single Atoms from Molten Salt for Facilitating Selective CO_2 Reduction, Adv. Mater. 36 (2024) e2406380.

[80] Z. Zhang, H. Li, Y. Shao, L. Gan, F. Kang, W. Duan, H.A. Hansen, J. Li, Molecular understanding of the critical role of alkali metal cations in initiating CO_2 electroreduction on Cu(100) surface, Nat. Commun. 15 (2024) 612.

[81] Z.-M. Zhang, T. Wang, Y.-C. Cai, X.-Y. Li, J.-Y. Ye, Y. Zhou, N. Tian, Z.-Y. Zhou, S.-G. Sun, Probing electrolyte effects on cation-enhanced CO_2 reduction on copper in acidic media, Nat. Catal. 7 (2024) 807–817.

[82] Y. Wang, J. Zhang, J. Zhao, Y. Wei, S. Chen, H. Zhao, Y. Su, S. Ding, C. Xiao, Strong Hydrogen-Bonded Interfacial Water Inhibiting Hydrogen Evolution Kinetics to Promote Electrochemical CO_2 Reduction to C_2^+, ACS Catal. 14 (2024) 3457–3465.

[83] Y.-m Wang, H.-M. Yan, H. Cao, J.-w Chen, H. Yang, J.-y Zhu, J. Sun, Atomic-Scale Understanding of Electrified Interfacial Structures and Dynamics during the Oxygen Reduction Reaction on the Fe–N_4/C Electrocatalyst, ACS Catal. 13 (2023) 11080–11090.

[84] H.M. Yan, G. Wang, X.M. Lv, H. Cao, G.Q. Qin, Y.G. Wang, Revealing the Potential-Dependent Rate-Determining Step of Oxygen Reduction Reaction on Single-Atom Catalysts, J. Am. Chem. Soc. 147 (2025) 3724–3730.

[85] S. Choi, H. Lee, J. Kwon, J. Sun, G. Ali, L. Olivi, N. Imam, J. Choi, J.H. Kim, H. Han, Elucidating mechanism of Se-induced lattice oxygen activation and structural stability in perovskite oxide for oxygen evolution catalysis, J. Power Sources 657 (2025) 238152.

[86] S. Wei, Y. Luo, H. Zhang, X. Du, Y. Wang, G. Liu, J. Li, Voltage-Dependent Electrochemical Carbon Dioxide Reduction Mechanism Unveiled by Kinetic Monte Carlo Simulation, J. Phys. Chem. Lett. 16 (2025) 2896–2904.

[87] P. Lozano-Reis, P. Gamallo, R. Sayos, F. Illas, Comprehensive Density Functional and Kinetic Monte Carlo Study of CO_2 Hydrogenation on a Well-Defined Ni/CeO_2 Model Catalyst: Role of Eley-Rideal Reactions, ACS Catal. 14 (2024) 2284–2299.

[88] J. Meng, J. Freeze, L. Nowack, C. Li, H. Wang, H.D. Abruna, A.P. Willard, V. S. Batista, T. Lian, Competitive Carbonate Binding Hinders Electrochemical CO_2 Reduction to CO on Cu Surfaces at Low Overpotentials, J. Am. Chem. Soc. 147 (2025) 25361–25371.

[89] Y. Fan, X. Wang, G. Bo, X. Xu, K.W. See, B. Johannessen, W.K. Pang, Operando Synchrotron X-Ray Absorption Spectroscopy: A Key Tool for Cathode Material Studies in Next-Generation Batteries, Adv. Sci. 12 (2025) 2414480.

[90] L. Chen, X. Ding, Z. Wang, S. Xu, Q. Jiang, C. Dun, J.J. Urban, Advances in in situ/operando techniques for catalysis research: enhancing insights and discoveries, Surf. Sci. Technol. 2 (2024) 9.

[91] J. Timoshenko, F.T. Haase, S. Saddeler, M. Rüscher, H.S. Jeon, A. Herzog, U. Hejral, A. Bergmann, S. Schulz, B. Roldan Cuenya, Deciphering the structural and chemical transformations of oxide catalysts during oxygen evolution reaction using quick X-ray absorption spectroscopy and machine learning, J. Am. Chem. Soc. 145 (2023) 4065–4080.

[92] J. Timoshenko, A.I. Frenkel, Inverting" X-ray absorption spectra of catalysts by machine learning in search for activity descriptors, Acs Catal. 9 (2019) 10192–10211.

[93] V.H. Do, J.M. Lee, Transforming adsorbate surface dynamics in aqueous electrocatalysis: pathways to unconstrained performance, Adv. Mater. 37 (2025) 2417516.

[94] Y. Zhou, J. Zeng, X. Zheng, W. Huang, Y. Dong, J. Zhang, Y. Deng, R. Wu, Enhancing the oxygen evolution reaction activity and stability of high-valent CoOOH by switching the catalytic pathway through doping low-valent Cu, J. Colloid Interface Sci. 678 (2025) 536–546.

[95] Y. He, M. Wang, H. Ji, Q. Cheng, S. Liu, Y. Huan, T. Qian, C. Yan, Molecular Dynamics Simulations for Electrocatalytic CO_2 Reduction: Bridging Macroscopic Experimental Observations and Microscopic Explanatory Mechanisms, Adv. Funct. Mater. 35 (2024) 2413703.

[96] Y. Wang, J.M. Lamim Ribeiro, P. Tiwary, Machine learning approaches for analyzing and enhancing molecular dynamics simulations, Curr. Opin. Struct. Biol. 61 (2020) 139–145.

[97] N. Yao, X. Chen, Z.H. Fu, Q. Zhang, Applying Classical, Ab Initio, and Machine-Learning Molecular Dynamics Simulations to the Liquid Electrolyte for Rechargeable Batteries, Chem. Rev. 122 (2022) 10970–11021.

[98] H. Li, Y. Jiao, K. Davey, S.Z. Qiao, Data-Driven Machine Learning for Understanding Surface Structures of Heterogeneous Catalysts, Angew. Chem. Int Ed. Engl. 62 (2023) e202216383.

[99] G.E. Hinton, R.R. Salakhutdinov, Reducing the dimensionality of data with neural networks, science 313 (2006) 504–507.

[100] Y. LeCun, Y. Bengio, G. Hinton, Deep learning, nature 521 (2015) 436–444.

[101] A.K. Jain, M.N. Murty, P.J. Flynn, Data clustering: a review, ACM Comput. Surv. (CSUR) 31 (1999) 264–323.

[102] L. Zhang, J. Han, H. Wang, R. Car, E. W, Deep potential molecular dynamics: a scalable model with the accuracy of quantum mechanics, Phys. Rev. Lett. 120 (2018) 143001.

[103] J. Behler, M. Parrinello, Generalized neural-network representation of high-dimensional potential-energy surfaces, Phys. Rev. Lett. 98 (2007) 146401.

[104] K.T. Schütt, H.E. Sauceda, P.-J. Kindermans, A. Tkatchenko, K.-R. Müller, Schnet–a deep learning architecture for molecules and materials, J. Chem. Phys. 148 (2018) 241722.

[105] J. Gasteiger, J. Groß, S. Günnemann, Directional Message passing for Molecular Graphs,arXiv preprint arXiv:2003.03123, (2020).

[106] T. Lookman, P.V. Balachandran, D. Xue, R. Yuan, Active learning in materials science with emphasis on adaptive sampling using uncertainties for targeted design, npj Comput. Mater. 5 (2019) 21.

[107] Z. Ghahramani, Probabilistic machine learning and artificial intelligence, Nature 521 (2015) 452–459.
[108] D.P. Kingma, M. Welling, Auto-encoding variational bayes, arXiv preprint arXiv: 1312.6114, (2013).
[109] J. Ho, A. Jain, P. Abbeel, Denoising diffusion probabilistic models, Adv. Neural Inf. Process. Syst. 33 (2020) 6840–6851.
[110] R.S. Sutton, A.G. Barto. Reinforment Learning: An Introduction, 2nd ed, MIT, Press, Cambridge, MA, 2018.
[111] J.H. Jensen, A graph-based genetic algorithm and generative model/Monte Carlo tree search for the exploration of chemical space, Chem. Sci. 10 (2019) 3567–3572.
[112] K. Champion, B. Lusch, J.N. Kutz, S.L. Brunton, Data-driven discovery of coordinates and governing equations, Proc. Natl. Acad. Sci. 116 (2019) 22445–22451.
[113] Z.C. Lipton, The mythos of model interpretability: In machine learning, the concept of interpretability is both important and slippery, Queue 16 (2018) 31–57.
[114] Z.W. Seh, J. Kibsgaard, C.F. Dickens, I. Chorkendorff, J.K. Nørskov, T. F. Jaramillo, Combining theory and experiment in electrocatalysis: Insights into materials design, Science 355 (2017) eaad4998.
[115] J. Graciani, K. Mudiyanselage, F. Xu, A.E. Baber, J. Evans, S.D. Senanayake, D. J. Stacchiola, P. Liu, J. Hrbek, J.F. Sanz, Highly active copper-ceria and copper-ceria-titania catalysts for methanol synthesis from CO2, Science 345 (2014) 546–550.
[116] J. Schmidt, M.R. Marques, S. Botti, M.A. Marques, Recent advances and applications of machine learning in solid-state materials science, npj Comput. Mater. 5 (2019) 83.
[117] C.R. Harris, K.J. Millman, S.J. Van Der Walt, R. Gommers, P. Virtanen, D. Cournapeau, E. Wieser, J. Taylor, S. Berg, N.J. Smith, Array programming with NumPy, nature 585 (2020) 357–362.
[118] R. Guidotti, A. Monreale, S. Ruggieri, F. Turini, F. Giannotti, D. Pedreschi, A survey of methods for explaining black box models, ACM Comput. Surv. (CSUR) 51 (2018) 1–42.
[119] P.L. Bartlett, P.M. Long, G. Lugosi, A. Tsigler, Benign overfitting in linear regression, Proc. Natl. Acad. Sci. 117 (2020) 30063–30070.
[120] C. Rudin, Stop explaining black box machine learning models for high stakes decisions and use interpretable models instead, Nat. Mach. Intell. 1 (2019) 206–215.
[121] J. Sun, J. Yu, Y. Guo, Q. Wang, Enhancing power factor of SnSe sheet with grain boundary by doping germanium or silicon, NPJ Comput. Mater. 6 (2020) 99.
[122] S. Cuomo, V.S. Di Cola, F. Giampaolo, G. Rozza, M. Raissi, F. Piccialli, Scientific machine learning through physics–informed neural networks: Where we are and what's next, J. Sci. Comput. 92 (2022) 88.
[123] M. Raissi, P. Perdikaris, G.E. Karniadakis, Physics-informed neural networks: A deep learning framework for solving forward and inverse problems involving nonlinear partial differential equations, J. Comput. Phys. 378 (2019) 686–707.
[124] S.N. Steinmann, Q. Wang, Z.W. Seh, How machine learning can accelerate electrocatalysis discovery and optimization, Mater. Horiz. 10 (2023) 393–406.
[125] H. Chen, E. Kätelhön, Y. Lu, J. Cheng, Z.-Q. Tian, R.G. Compton, 30 years AI Electro. Where we are what's. ? eScience 6 (2025) 100515.
[126] T. Binninger, R. Mohamed, K. Waltar, E. Fabbri, P. Levecque, R. Kötz, T. J. Schmidt, Thermodynamic explanation of the universal correlation between oxygen evolution activity and corrosion of oxide catalysts, Sci. Rep. 5 (2015) 12167.
[127] L. Yao, Z. Ou, B. Luo, C. Xu, Q. Chen, Machine Learning to Reveal Nanoparticle Dynamics from Liquid-Phase TEM Videos, ACS Cent. Sci. 6 (2020) 1421–1430.
[128] Y. Sun, X. Zhang, R. Huang, D. Yang, J. Kim, J. Chen, E.H. Ang, M. Li, L. Li, X. Song, Revealing microscopic dynamics: in situ liquid-phase TEM for live observations of soft materials and quantitative analysis via deep learning, Nanoscale 16 (2024) 2945–2954.
[129] S. Lee, S.M. Ribet, A.R. McCray, A. Barnum, J.A. Dionne, C. Ophus, Unsupervised clustering algorithm for efficient processing of 4D-STEM and 5D-STEM data, arXiv, 2601 (2026) 17262.
[130] X. Wang, J. Li, H.D. Ha, J.C. Dahl, J.C. Ondry, I. Moreno-Hernandez, T. Head-Gordon, A.P. Alivisatos, AutoDetect-mNP: An Unsupervised Machine Learning Algorithm for Automated Analysis of Transmission Electron Microscope Images of Metal Nanoparticles, JACS Au 1 (2021) 316–327.
[131] M. Scott, Unsupervised Machine Learning Analysis for 4D-STEM Datasets, Microsc. Microanal. 30 (2024) 119.
[132] Y. Yang, C. Shi, J. Feijoo, J. Jin, C. Chen, Y. Han, P. Yang, Dynamic Evolution of Copper Nanowires during CO_2 Reduction Probed by Operando Electrochemical 4D-STEM and X-ray Spectroscopy, J. Am. Chem. Soc. 146 (2024) 23398–23405.
[133] X. Duan, H. Sun, S. Wang, Metal-free carbocatalysis in advanced oxidation reactions, Acc. Chem. Res. 51 (2018) 678–687.
[134] M. Williamson, R. Tromp, P. Vereecken, R. Hull, iF. Ross, Dynamic microscopy of nanoscale cluster growth at the solid–liquid interface, Nat. Mater. 2 (2003) 532–536.
[135] A. Voronov, A. Urakawa, W. van Beek, N.E. Tsakoumis, H. Emerich, M. Ronning, Multivariate curve resolution applied to in situ X-ray absorption spectroscopy data: an efficient tool for data processing and analysis, Anal. Chim. Acta 840 (2014) 20–27.
[136] W.H. Cassinelli, L. Martins, A.R. Passos, S.H. Pulcinelli, C.V. Santilli, A. Rochet, V. Briois, Multivariate curve resolution analysis applied to time-resolved synchrotron X-ray Absorption Spectroscopy monitoring of the activation of copper alumina catalyst, Catal. Today 229 (2014) 114–122.
[137] A. Martini, E. Borfecchia, Spectral Decomposition of X-ray Absorption Spectroscopy Datasets: Methods and Applications, Crystals 10 (2020) 664.
[138] A. Martini, D. Hursan, J. Timoshenko, M. Ruscher, F. Haase, C. Rettenmaier, E. Ortega, A. Etxebarria, B.Roldan Cuenya, Tracking the Evolution of Single-Atom Catalysts for the CO_2 Electrocatalytic Reduction Using Operando X-ray Absorption Spectroscopy and Machine Learning, J. Am. Chem. Soc. 145 (2023) 17351–17366.
[139] A. Vladyka, C.J. Sahle, J. Niskanen, Towards structural reconstruction from X-ray spectra, Phys. Chem. Chem. Phys. 25 (2023) 6707–6713.
[140] D. Shin, J. Kim, C. Kim, K. Bae, S. Baek, G. Kang, Y. Urzhumov, D.R. Smith, K. Kim, Scalable variable-index elasto-optic metamaterials for macroscopic optical components and devices, Nat. Commun. 8 (2017) 16090.
[141] A. Martini, J. Timoshenko, M. Ruscher, D. Hursan, M.C.O. Monteiro, E. Liberra, B. Roldan Cuenya, Revealing the structure of the active sites for the electrocatalytic CO_2 reduction to CO over Co single atom catalysts using operando XANES and machine learning, J. Synchrotron Radiat. 31 (2024) 741–750.
[142] M. Ruscher, A. Herzog, J. Timoshenko, H.S. Jeon, W. Frandsen, S. Kuhl, B. Roldan Cuenya, Tracking heterogeneous structural motifs and the redox behaviour of copper-zinc nanocatalysts for the electrocatalytic CO_2 reduction using operando time resolved spectroscopy and machine learning, Catal. Sci. Technol. 12 (2022) 3028–3043.
[143] S. Srivastava, W. Wang, W. Zhou, M. Jin, P.J. Vikesland, Machine learning-assisted surface-enhanced Raman spectroscopy detection for environmental applications: a review, Environ. Sci. & Technol. 58 (2024) 20830–20848.
[144] Y. Xue, L. Zhang, G. Zheng, Recent Advances in CO_2 Electroreduction Driven by Artificial Intelligence and Machine Learning, Adv. Energy Mater. 15 (2025) e03560.
[145] T. Ying, R. Zhu, Y. Wang, Y. Zhu, Artificial Intelligence Guided Single Atom Catalysts: From Precise Design to Industrial-Grade Preparation, Adv. Funct. Mater. 36 (2025) e15026.
[146] J. Wei, S. Yu, T. Zhou, J. Shang, S. Liu, F. Han, X. Li, Q. An, situ SERS and in situ Raman: deciphering interfacial phenomena and processes, Mater. Horiz. 12 (2025) 9381–9415.
[147] F.-T. Wang, J. Cheng, Investigating water structure and dynamics at metal/water interfaces from classical, ab initio to machine learning molecular dynamics, Curr. Opin. Electrochem. 49 (2025) 101605.
[148] T. Wang, Q. Wu, Y. Han, Z. Guo, J. Chen, C. Liu, Advanced theoretical modeling methodologies for electrocatalyst design in sustainable energy conversion, Appl. Phys. Rev. 12 (2025) 011316.
[149] B. Li, S.D. Jiang, Q. Fu, R. Wang, W.Z. Xu, J.X. Chen, C. Liu, P. Xu, X.J. Wang, J. H. Li, H.B. Fan, J.T. Huo, J.F. Sun, Z.L. Ning, B. Song, Tailoring Nanocrystalline/Amorphous Interfaces to Enhance Oxygen Evolution Reaction Performance for FeNi-Based Alloy Fibers, Adv. Funct. Mater. 35 (2024) 2413088.
[150] Y. Huang, S.H. Wang, X. Wang, N. Omidvar, L.E.K. Achenie, S.E. Skrabalak, H. Xin, Unraveling Reactivity Origin of Oxygen Reduction at High-Entropy Alloy Electrocatalysts with a Computational and Data-Driven Approach, J. Phys. Chem. C. Nanomater Interfaces 128 (2024) 11183–11189.
[151] L. Wu, T. Guo, T. Li, Rational design of transition metal single-atom electrocatalysts: a simulation-based, machine learning-accelerated study, J. Mater. Chem. A 8 (2020) 19290–19299.
[152] F. Noe, A. Tkatchenko, K.R. Muller, C. Clementi, Machine Learning for Molecular Simulation, Annu Rev. Phys. Chem. 71 (2020) 361–390.
[153] H. Chan, B. Narayanan, M.J. Cherukara, F.G. Sen, K. Sasikumar, S.K. Gray, M.K. Y. Chan, S.K.R.S. Sankaranarayanan, Machine Learning Classical Interatomic Potentials for Molecular Dynamics from First-Principles Training Data, J. Phys. Chem. C. 123 (2019) 6941–6957.
[154] P. Pattnaik, S. Raghunathan, T. Kalluri, P. Bhimalapuram, C.V. Jawahar, U. D. Priyakumar, Machine Learning for Accurate Force Calculations in Molecular Dynamics Simulations, J. Phys. Chem. A 124 (2020) 6954–6967.
[155] Q. Yu, P. Li, X. Ni, Y. Li, L. Wang, Dynamics and kinetics exploration of the oxygen reduction reaction at the Fe-N_4/C-water interface accelerated by a machine learning force field, Chem. Sci. 16 (2025) 3620–3629.
[156] J. Jung, S. Ju, P.-h Kim, D. Hong, W. Jeong, J. Lee, S. Han, S. Kang, Electrochemical Degradation of Pt_3Co Nanoparticles Investigated by Off-Lattice Kinetic Monte Carlo Simulations with Machine-Learned Potentials, ACS Catal. 13 (2023) 16078–16087.
[157] M. Sun, B. Jin, X. Yang, S. Xu, Probing nuclear quantum effects in electrocatalysis via a machine-learning enhanced grand canonical constant potential approach, Nat. Commun. 16 (2025) 3600.
[158] J.L. Li, Y.F. Li, Z.P. Liu, Situ Structure of a Mo-Doped Pt-Ni catalyst during electrochemical oxygen reduction resolved from machine learning-based grand canonical global optimization, JACS Au 3 (2023) 1162–1175.
[159] S. Han, S. De, Machine learning-accelerated, evolutionary Monte Carlo for rapid phase exploration of compositionally complex materials in reactive environments, ChemRxiv, 2025.
[160] C. Yang, X. Fu, D. Luan, J. Xiao, Towards rational design of confined catalysis in carbon nanotube by machine learning and grand canonical Monte Carlo simulations, Angew. Chem. Int Ed. Engl. 64 (2024) e202421552.